and $(DEA)_2CoCl_4$, the entropy change can be accounted for by a simple 2-fold disorder of the cation. In contrast, the ΔS_{tr} values for $(DEA)_2ZnCl_4 \cdot xH_2O$ and $(DEA)_2MnCl_4$ indicate more disorder, probably due to disorder of the ethyl groups. This is consistent with the structural results on the partially hydrated Zn^{2+} salts. The three $(CH_3)_2CHNH_3^+$ salts listed are all thermochromic and their phase transitions have been investigated in some detail.[9-11] The two trihalide compounds are both linear chain compounds, and the phase transitions (the lower temperature one, in the case of the bromide) involve a rearrangement of the chain structure and the onset of a 2-fold disorder of the cation in the higher temperature phase. The ΔS_{tr} values are substantially larger than R ln 2 and the excess entropy is associated with rearrangement of the chain structure. The low-temperature phase of the tetrahalide salt is a complicated chain structure involving $CuCl_4^{2-}$ anions linked by semicoordinate Cu···Cl linkages. The high-temperature phase consists of isolated distorted terahedral $CuCl_4^{2-}$ anions again with a 2-fold disorder of the cations. Again, the ΔS_{tr} value is substantially larger than the $2R$ ln 2 value. The thermal ellipsoids indicate some substantial amount of librational motion for the anions, but no detailed analysis was made. Nevertheless, the ΔS_{tr} value is not as large as that reported for $(DEA)_2CuCl_4$ in this study, in accord with the large amount of thermal motion observed for both the cations and anions. The temperature dependence of NMR line widths of the $(CH_3)_2CHNH_3^+$ salts was similar to that observed here, and the change in second moment at T_{tr} could be accounted for by the observed 2-fold disorder of the cation. No unusual temperature dependence was observed for the EPR line widths either. This is in direct contrast to the observations for $(DEA)_2CuCl_4$, where the strong temperature dependence is evidence for temperature-dependent librational motion.

Acknowledgment. The support of PRF Grant 15813-AC6,3 is gratefully acknowledged. The X-ray facility was established through funds provided by NSF Grant CHE-8408407 and The Boeing Company.

Supplementary Material Available: Tables SI and SII listing thermal parameters and derived hydrogen atom positions and Figure SI giving the unit cell packing diagram (4 pages); tables of calculated and observed structure factors (20 pages). Ordering information is given on any current masthead page.

Synthesis, Crystal Structures, Reactivity, and Magnetochemistry of a Series of Binuclear Complexes of Manganese(II), -(III), and -(IV) of Biological Relevance. The Crystal Structure of $[L'Mn^{IV}(\mu\text{-}O)_3Mn^{IV}L'](PF_6)_2 \cdot H_2O$ Containing an Unprecedented Short Mn···Mn Distance of 2.296 Å

Karl Wieghardt,*[1a] Ursula Bossek,[1a] Bernhard Nuber,[1b] Johannes Weiss,[1b] J. Bonvoisin,[1c] M. Corbella,[1c] S. E. Vitols,[1c] and J. J. Girerd*[1c]

Contribution from the Lehrstuhl für Anorganische Chemie I, Ruhr-Universität, D-4630 Bochum, FRG, the Anorganisch-chemisches Institut der Universität, 6900 Heidelberg, FRG, and the Laboratoire de Spectrochimie des Elements de Transition, UA CNRS 420, Université de Paris-Sud, 91405 Orsay, France. *Received March 15, 1988*

Abstract: The disproportionation reactions of two binuclear complexes of manganese(III) containing the oxo-bis(acetato)-dimanganese(III) core and two 1,4,7-triazacyclononane (L) capping ligands (**1**) or two *N,N',N''*-trimethyl-1,4,7-triazacyclononane (L') ligands (**2**) in aqueous solution under anaerobic conditions lead to a variety of novel binuclear $Mn^{III}Mn^{IV}$ and Mn^{IV}_2 dimers. These are the following: $[L_2Mn^{III}Mn^{IV}(\mu\text{-}O)_2(\mu\text{-}CH_3CO_2)][BPh_4]_2 \cdot CH_3CN$ (**5**); $[L'_2Mn^{III}Mn^{IV}(\mu\text{-}O)(\mu\text{-}CH_3CO_2)_2](ClO_4)_3$ (**6**); $[L_2Mn^{IV}_2(OH)_2(\mu\text{-}O)_2][Mn^{II}_3(C_2O_4)_4(OH_2)_2] \cdot 6H_2O$ (**7**); and $[L'_2Mn^{IV}_2(\mu\text{-}O)_3](PF_6)_2 \cdot H_2O$ (**9**). A tetranuclear species $[L_4Mn^{IV}_4O_6]Br_4 \cdot 5.5H_2O$ (**8**) is generated as a thermodynamically very stable product from a Mn^{II} containing aqueous solution of L in the presence of oxygen. In the absence of oxygen methanolic solutions of $Mn(ClO_4)_2 \cdot 2H_2O$ or manganese(II) acetate react with L' to form $[L'_2Mn^{II}_2(\mu\text{-}OH)(\mu\text{-}CH_3CO_2)_2](ClO_4)$ (**3**) and $[L'_2Mn^{II}_2(\mu\text{-}CH_3CO_2)_3][BPh_4]$ (**4**). The oxo- and acetato-bridges in **1** and **2** are labile; addition of anions X^- (X = Cl, Br, NCS, N_3) to acetonitrile solutions of **1** or **2** yields the monomers $LMnX_3$ and $L'MnX_3$. The electrochemistry of all compounds has been investigated; for example, **2** is reversibly oxidized by two one-electron processes to generate $Mn^{III}Mn^{IV}$ and Mn^{IV}_2 dimers in liquid SO_2. The crystal structures of **4**, **7**, **8**, and **9** have been determined by X-ray crystallography: **4**, orthorhombic *Pcab*, a = 17.368 (5) Å, b = 17.538 (5) Å, c = 33.21 (1) Å, Z = 8; **7**, monoclinic $C2/c$, a = 13.391 (3) Å, b = 16.571 (4) Å, c = 19.312 (4) Å, β = 109.82 (2)°, Z = 4; **8**, monoclinic $P2_1/c$, a = 17.548 (8) Å, b = 13.118 (7) Å, c = 21.56 (1) Å, β = 105.63 (4)°, Z = 4; **9**, orthorhombic *Pnma*, a = 10.057 (5) Å, b = 16.12 (1) Å, c = 19.237 (8) Å, Z = 4. **9** consists of the cofacial bioctahedral cation $(L'Mn^{IV}(\mu\text{-}O)_3Mn^{IV}L']^{2+}$ and PF_6 anions. The Mn···Mn distance is unusually short (2.296 (2) Å). Bulk magnetic properties of all compounds have been studied between 100 and 298 K, and in some instances 4 and 298 K. In **2** the Mn(III) ions are ferromagnetically coupled, J = +18 (1) cm^{-1}; whereas the Mn^{II} centers in **4** are weakly antiferromagnetically coupled, J = -3.5 (2) cm^{-1}. Very strong intramolecular antiferromagnetic coupling is observed in **9** (J = -780 cm^{-1}).

It is well established that manganese is an essential trace element in biology.[2] The oxidation of water by photosynthetic enzymes (photosystem II; PS II),[3] the reduction of ribonucleotides in certain bacteria,[4] and the disproportionation of hydrogen

0002-7863/88/1510-7398$01.50/0

peroxide by some catalases or pseudocatalases[5] have been shown to occur at bi- or polynuclear manganese containing active sites. These and other studies have in recent years revived an intense research in the area of classical Werner-type coordination chemistry of manganese. Special emphasis has been placed on the preparation and structural characterization of dimeric and oligomeric compounds containing manganese centers in the higher oxidation states III and IV. The spectroscopic and magnetic properties of these complexes are compared with those of the biomolecules. Thus the aim of this work is to provide corroborative and speculative model compounds[6] with well understood structural and electronic properties.

We have recently reported[7] the facile synthesis of two binuclear manganese(III) compounds via spontaneous self-assembly, **1** and **2**, containing the (μ-oxo)-bis(μ-carboxylato)dimanganese(III) core and the macrocycle 1,4,7-triazacyclononane (L) or *N,N',N''*-trimethyl-1,4,7-triazacyclononane (L') as tridentate capping ligands at each Mn(III). Dismukes, Lippard, and co-workers[8] have reported similar neutral compounds using hydro-tris(1-pyrazolyl)borate as the capping ligand.

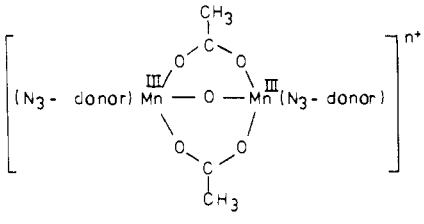

N_3 - donor 1,4,7- triazacyclononane, n = 2 **1**

N,N',N''- trimethyl- 1,4,7- triazacyclononane, n = 2 **2**

hydro(trispyrazolyl)borate(1-), n = 0

Both the positions and relative intensities of the absorption maxima in the visible region of **1**, **2**, and their hydro-tris(1-pyrazolyl)borate analogues are very similar to those published for the two manganese centers per subunit containing pseudocatalase from *Lactobacillus plantarum*.[5] Therefore, a binuclear μ-oxo-bis(μ-carboxylato)dimanganese(III) unit may be envisaged in this enzyme.[8,9] The same appears to be true for a recently characterized ribonucleotide reductase from *Brevibacterium ammoniagenes*.[4c]

We here wish to report the rich redox chemistry of **1** and **2** and their interesting reactivity in aqueous solution. **1** and **2** undergo a series of disproportionation reactions in aqueous solution and a variety of different reaction products may be isolated. Preliminary reports on some aspects of this work have been published.[9-13] Thermodynamically, a tetranuclear species, $[L_4Mn_4O_6]^{4+}$, with an adamantane-like $\{Mn_4O_6\}^{4+}$ skeleton is the most stable species in alkaline aqueous solutions of 1,4,7-triazacyclononane and manganese(II) in the presence of oxygen.[13] We here report full details of the X-ray structure determination of $[L_4Mn_4O_6]Br_4 \cdot 5.5H_2O$[13] and its magnetic properties. Tetranuclear manganese complexes[13-15] are of current interest as model compounds for the manganese cluster in the water splitting enzyme PS II for which physical evidence for four manganese centers per active site has been reported recently.[16-19]

Experimental Section

The tridentate ligands 1,4,7-triazacyclononane (L)[20] and *N,N',N''*-trimethyl-1,4,7-triazacyclononane (L')[21] were prepared as described in the literature.

$[L_2Mn^{III}_2(\mu\text{-}O)(\mu\text{-}CH_3CO_2)_2](ClO_4)_2$ (**1**) and $[L'_2Mn^{III}_2(\mu\text{-}O)(\mu\text{-}CH_3CO_2)_2](ClO_4)_2 \cdot H_2O$ (**2**) were prepared according to the literature.[7]

$[L'_2Mn^{II}_2(\mu\text{-}OH)(\mu\text{-}CH_3CO_2)_2](ClO_4)$ (3). To a solution of *N,N',N''*-trimethyl-1,4,7-triazacyclononane (1 g; 5.8 mmol) in anhydrous methanol (30 mL) under an argon atmosphere was added $Mn(ClO_4)_2 \cdot 6H_2O$ (0.5 g; 1.38 mmol). After the solution was stirred for 1 h at room temperature sodium acetate (0.25 g, 3.0 mmol) was added, and the volume of the solution was then slowly reduced to 20 mL by passage of a stream of argon through this solution. On storage at 0 °C for 2-3 days transparent pale-blue to colorless crystals of **3** precipitated, which were filtered off and dried under argon (yield: 0.7 g).

Anal. Calcd for $C_{22}H_{49}N_6Mn_2ClO_9$: C, 38.46; H, 7.19; N, 12.23; ClO_4, 14.48. Found: C, 38.2; H, 7.3; N, 12.2; ClO_4, 14.3. IR (KBr, cm^{-1}): ν(OH) 3520; ν(C-O) 1615 (vs), 1405 (vs).

$[L'_2Mn^{II}_2(\mu\text{-}CH_3CO_2)_3][BPh_4]$ (4). To an argon-scrubbed solution of *N,N',N''*-trimethyl-1,4,7-triazacyclononane (0.5 g; 12.9 mmol) in methanol (30 mL), manganese(II) acetate tetrahydrate (0.6 g; 2.4 mmol) was added. After the clear, colorless solution was stirred for 15 min at 20 °C, sodium tetraphenylborate (0.4 g; 1.2 mmol) was added. Colorless microcrystals precipitated immediately. Recrystallization from a minimum amount of CH_3CN at 0 °C produced crystals of X-ray quality within 3 days (yield: 1.5 g).

Anal. Calcd for $C_{48}H_{71}N_6Mn_2O_6B$: C, 60.57; H, 7.52; N, 8.83. Found: C, 60.7; H, 7.4; N, 8.8. IR (KBr, cm^{-1}): ν(CO): 1636 (vs); 1423 (s).

$[L'_2Mn^{III}Mn^{IV}(\mu\text{-}O)(\mu\text{-}CH_3CO_2)_2](ClO_4)_3$ (6). To a solution of *N,N',N''*-trimethyl-1,4,7-triazacyclononane (1.0 g, 5.8 mmol) in ethanol (30 mL) under an argon atmosphere were added at room temperature manganese(III) acetate (1.5 g; 6.46 mmol), sodium acetate (1 g, 12 mmol), and water (20 mL). To this red-brown solution concentrated perchloric acid (2 mL) was added which initiated the precipitation of green-brown crystals of **6** (yield: 3.5 g). Larger crystals suitable for

(1) (a) Ruhr-Universität Bochum. (b) Universität Heidelberg. (c) Université de Paris-Sud.

(2) (a) Keen, C. L.; Lönnerdal, B.; Hurley, L. S. In *Biochemistry of the Essential Ultratrace Elements*; Frieden, E., Ed.; Plenum: New York and London, 1984; p 89. (b) *Manganese in Metabolism and Enzyme Function*; Schram, C. L., Wedler, F. C., Eds.; Academic: New York, 1986.

(3) Recent review articles focussing on the role of the manganese cluster: (a) Amesz, J. *Biochim. Biophys. Acta* **1983**, *726*, 1-12. (b) Renger, G.; Govindjee *Photosynth. Res.* **1985**, *6*, 33-55. (c) Webber, A. N.; Spencer, L.; Sawyer, D. T.; Heath, R. L. *FEBS Lett.* **1985**, *189*, 258-262. (d) Vincent, J. B.; Christou, G. *FEBS Lett.* **1986**, *207*, 250-252. (e) Witt, H. T.; Schlodder, E.; Brettel, K.; Saygin, Ö. *Ber. Bunsenges. Phys. Chem.* **1986**, *90*, 1015-1024. (f) Dismukes, G. C. *Photochem. Photobiol.* **1986**, *43*, 99. (g) Brudvig, G. W. *J. Bioenergetics Biomembranes* **1987**, *19*, 91-104. (h) Witt, H. T. *Nouv. J. Chim.* **1987**, *11*, 91-101. (i) dePaula, J. C.; Beck, W. T.; Brudvig, G. W. *Nouv. J. Chim.* **1987**, *11*, 103-107. (j) Renger, G. *Angew. Chem.* **1987**, *99*, 660-678; *Angew. Chem., Int. Ed. Engl.* **1987**, *26*, 643.

(4) (a) Schimpff-Weiland, G. S.; Follmann, H.; Auling, G. *Biochem. Biophys. Res. Commun.* **1981**, *102*, 1276. (b) Plönzig, J.; Auling, G. *Arch. Microbiol.* **1987**, *146*, 396-401. (c) Willing, A.; Follmann, H.; Auling, G. *Eur. J. Biochem.* **1988**, *170*, 603.

(5) (a) Kono, Y.; Fridovich, I. *J. Biol. Chem.* **1983**, *258*, 6015-6019, 13646-13648. (b) Beyer, W. F., Jr.; Fridovich, I. *Biochemistry* **1985**, *24*, 6460-6467.

(6) (a) Hill, H. A. O. *Chem. Br.* **1976**, *12*, 119-1213. (b) Ibers, J.; Holm, R. H. *Science* **1980**, *209*, 223.

(7) Wieghardt, K.; Bossek, U.; Ventur, D.; Weiss, J. *J. Chem. Soc., Chem. Commun.* **1985**, 347-349.

(8) Sheats, J. E.; Czernuszewicz, R. S.; Dismukes, G. C.; Rheingold, A. L.; Petrouleas, V.; Stubbe, J.; Armstrong, W. H.; Beer, R. H.; Lippard, S. J. *J. Am. Chem. Soc.* **1987**, *109*, 1435-1444.

(9) Wieghardt, K.; Bossek, U.; Bonvoisin, J.; Beauvillain, P.; Girerd, J. J.; Nuber, B.; Weiss, J.; Heinze, J. *Angew. Chem.* **1986**, *98*, 1026-1027; *Angew. Chem., Int. Ed. Engl.* **1986**, *25*, 1030-1031.

(10) Wieghardt, K.; Bossek, U.; Zsolnai, L.; Huttner, G.; Blondin, G.; Girerd, J. J.; Babonneau, F. *J. Chem. Soc., Chem. Commun.* **1987**, 651-653.

(11) Wieghardt, K.; Bossek, U.; Nuber, B.; Weiss, J. *J. Chem. Soc., Chem. Commun.*, submitted for publication.

(12) Wieghardt, K.; Bossek, U.; Nuber, B.; Weiss, J. *Inorg. Chim. Acta* **1987**, *126*, 39-43.

(13) Wieghardt, K.; Bossek, U.; Gebert, W. *Angew. Chem.* **1983**, *95*, 320; *Angew. Chem., Int. Ed. Engl.* **1983**, *22*, 328.

(14) McKee, V.; Shepard, W. B. *J. Chem. Soc., Chem. Commun.* **1985**, 158-159.

(15) (a) Vincent, J. B.; Christmas, C.; Huffman, J. C.; Christou, G.; Chang, H.-R.; Hendrickson, D. N. *J. Chem. Soc., Chem. Commun.* **1987**, 236-238. (b) Brooker, S.; McKee, V.; Shepard, W. B.; Pannell, L. *J. Chem. Soc., Dalton Trans.* **1987**, 2555.

(16) Murata, N.; Miyao, M.; Omata, T.; Matsunami, H.; Kuwabara, T. *Biochim. Biophys. Acta* **1984**, *765*, 363-369.

(17) dePaula, J. C.; Brudvig, G. W. *J. Am. Chem. Soc.* **1985**, *107*, 2643-2648.

(18) dePaula, J. C.; Beck, W. F.; Brudvig, G. W. *J. Am. Chem. Soc.* **1986**, *108*, 4002-4009.

(19) Beck, W. F.; dePaula, J. C.; Brudvig, G. W. *J. Am. Chem. Soc.* **1986**, *108*, 4018-4022.

(20) (a) Atkins, T. J.; Richman, J. E.; Oettle, W. F. *Org. Synth.* **1978**, *58*, 86. (b) Wieghardt, K.; Schmidt, W.; Nuber, B.; Weiss, J. *Chem. Ber.* **1979**, *112*, 2220.

(21) Wieghardt, K.; Chaudhuri, P.; Nuber, B.; Weiss, J. *Inorg. Chem.* **1982**, *21*, 3086.

Table I. Summary of Crystallographic Data and Data Collection

parameter	4	7	8	9
formula	$C_{48}H_{71}BMn_2N_6O_6$	$C_{20}H_{48}Mn_5N_6O_{36}$	$C_{24}H_{56}Br_4Mn_4N_{12}O_{11.5}$	$C_{18}H_{44}F_{12}Mn_2N_6O_4P_2$
space group	*Pcab*	*C2/c*	$P2_1/n$	*Pnma*
temp, K	298	295	295	298
a, Å	17.368 (5)	13.391 (3)	17.548 (8)	10.057 (5)
b, Å	17.538 (5)	16.571 (4)	13.118 (7)	16.12 (1)
c, Å	33.21 (1)	19.312 (4)	21.56 (1)	19.237 (8)
β, deg	90	109.82 (2)	105.63 (4)	
V, Å^3	10116 (2)	4031.5 (8)	4779.5 (8)	3118.7 (12)
d_{calcd}, g cm^{-3}	1.246	1.66	1.74	1.72
Z	8	4	4	4
FW	948.80	1095.32	1251.28	808.4
cryst size, mm	0.15 × 0.3 × 0.8	0.23 × 0.4 × 0.9	0.2 × 0.4 × 0.7	0.15 × 0.15 × 0.7
μ, cm^{-1}	5.3	12.2	43.6	9.8
radiation	graphite-monochromated Mo Kα($\lambda_{\bar{\alpha}}$ = 0.71073 Å)			
transmission coeff	0.80–1.00	0.84–1.00	0.60–1.00	0.88–1.00
scan type	ω	ω	θ–2θ	ϑ–ω
data collection range	$+h,+k,+l$ ($2° < 2\theta < 55°$)	$\pm h,+k,+l$ ($3° < 2\theta < 60°$)	$-h,-k,\pm l$ ($3° < 2\theta < 60°$)	$+h,+k,+l$ ($2.5 < 2\theta < 60°$)
no. of unique data	12000	~6000	~14000	4500
no. of data, $I > n\sigma(I)$	2428 (n = 2.5)	2524 (n = 2.5)	6391 (n = 2.0)	1404 (n = 2.5)
no. of variables	302	269	483	223
R_1[a]	0.074	0.057	0.061	0.066
R_2[b]	0.062	0.048	0.058	0.056
largest peak,[c] e$^-$/Å^3	0.5	0.65	2.6	0.6
Δ/σ[d]	0.51 (0.2)	0.18 (0.03)	0.07 (0.01)	0.05 (0.02)

[a] $R_1 = \sum||F_o| - |F_c||/\sum|F_o|$. [b] $R_2 = [\sum w(|F_o| - |F_c|)^2/\sum w|F_o|^2]^{1/2}$. [c] Largest peak in the final difference Fourier map. [d] Largest shift (Δ)-to-error (σ) ratio in the final least-squares cycle; mean value in brackets.

X-ray analysis were grown from an acetonitrile solution of **6** by addition of sodium perchlorate.

Anal. Calcd for $C_{22}H_{48}Cl_3Mn_2N_6O_{17}$: C, 29.86; H, 5.47; N, 9.50; ClO_4, 33.72. Found: C, 29.9; H, 5.4; N, 9.7; ClO_4, 33.5. IR (KBr, cm^{-1}): ν(CO) 1540 (vs); 1445, 1440 (s).

$[L_2Mn^{IV}_2(OH)_2(\mu\text{-}O)_2][Mn^{II}_3(C_2O_4)_4(OH_2)_2]\cdot 6H_2O$ (7). **1** (1.0 g; 1.43 mmol) dissolved under an argon atmosphere in water (30 mL) yielded a deep green solution to which sodium oxalate (1 g; 7.5 mmol) was added at room temperature. Green microcrystals of **7** precipitated immediately (yield: 0.8 g). Single crystals suitable for X-ray analysis were grown from an aqueous solution of **1** into which the solution containing the sodium oxalate was allowed to slowly diffuse within 24 h.

Anal. Calcd for $C_{20}H_{48}N_6O_{28}Mn_5$: C, 21.93; H, 4.41; N, 7.67; Mn, 25.08. Found: C, 22.2; H, 4.5; N, 7.7; Mn, 24.9. IR (KBr, cm^{-1}): $\nu(C_2O_4)$ 1615 (vs), 1590 (vs), 1580 (sh).

$[L'_2Mn^{IV}_2(\mu\text{-}O)_3](PF_6)_2\cdot H_2O$ (9). To **2** (0.5 g, 0.62 mmol) dissolved in a 1:1 H_2O/ethanol mixture (30 mL) was added triethylamine (3 mL). An immediate color change to brown was observed. To this solution was added $NaPF_6$ (2.0 g). Within a few minutes small amounts of MnO_2 precipitated, which was filtered off. From the resulting solution large red crystals of **9** precipitated (yield: 0.4 g).

Anal. Calcd for $C_{18}H_{42}N_6O_3Mn_2P_2F_{12}$: C, 26.74; H, 5.49; N, 10.40. Found: C, 26.5; H, 5.4; N, 10.4.

$L'Mn^{III}X_3$ (X = Cl, NCS, N_3). $L'MnCl_3$ was obtained as deep-red microcrystalline solid from a solution of **2** (1 g, 1.24 mmol) in CH_3CN to which 10 drops of concentrated hydrochloric acid were added at 20 °C (yield: 0.25 g).

Anal. Calcd for $C_9H_{21}N_3MnCl_3$: C, 32.50; H, 6.36; N, 12.63. Found: C, 32.3; H, 6.5; N, 12.4.

$L'Mn(NCS)_3$ or $L'Mn(N_3)_3$ were obtained as black-red microcrystals from an ethanolic solution (40 mL) of **2** (0.5 g; 0.62 mmol) to which 2 mL of water were added by addition of NaSCN (0.5 g) or NaN_3 (0.5 g).

Anal. Calcd for $C_{12}H_{21}N_6MnS_3$: C, 36.00; H, 5.29; N, 21.00. Found: C, 35.8; H, 5.4; N, 20.8. IR (KBr, cm^{-1}): ν(NCS) 2050 (vs).

Anal. Calcd for $C_9H_{21}N_{12}Mn$: C, 30.69; H, 6.01; N, 47.71. Found: C, 30.4; H, 5.8; N, 47.5. IR (KBr, cm^{-1}): $\nu(N_3)$ 2063 (vs), 2026 (vs).

The corresponding complexes containing 1,4,7-triazacyclononane as ligand may be prepared analogously.

Physical Measurements. Electrochemistry. Electrochemical experiments were performed with a Princeton Applied Research (PAR) Model 173 potentiostat, a PAR Model 175 universal programmer, a Model 179 digital coulometer, and a Kipp & Zonen X-Y recorder. Electrochemical measurements were made on acetonitrile solutions containing 0.1 M tetra-*n*-butylammonium hexafluorophosphate ($TBAPF_6$) as supporting electrolyte and were conducted at room temperature under an argon atmosphere. A standard three-electrode system was used for cyclic voltammetry (CV) experiments comprising a glassy carbon or platinum button working electrode, a platinum auxiliary electrode, and an Ag/AgCl (saturated LiCl in ethanol) electrode. The performance of the reference electrode was monitored by measuring the Cr(1+/0) couple of bis(diphenyl)chromium(I) tetrafluoroborate (BCr) (-0.586 V vs Ag/AgCl) or the Fe(+/0) couple of ferrocene (+0.537 V vs Ag/AgCl).[22]

Optical and Infrared Spectroscopy. Electronic absorption in the 200–1500 nm range was recorded with a Perkin-Elmer LAMBDA 9 spectrophotometer, while the infrared spectra (KBr-disks) were recorded with a Perkin-Elmer Model 283 B spectrometer.

Magnetic Susceptibility Measurements. Solid-state magnetic susceptibilities of powdered samples were measured with a Faraday-type magnetic balance (Bruker research magnet, Satorius microbalance) in the temperature range 100–298 K. In the temperature range 2.5–298 K a different Faraday-type magnetometer equipped with a helium continuous-flow cryostat was used. Independence of the magnetic susceptibility of the magnetic field was only checked for complexes **2**, **4**, and **8** at ambient temperature. $HgCo(SCN)_4$ was used as a susceptibility standard. Diamagnetic corrections were estimated from tabulated data (Pascal's constants[23]). The data reported here for the above three compounds correspond to low-field measurements (1 kG).

X-ray Crystallography. Intensities and lattice parameters of a colorless, tabular-shaped crystal of **4**, a dark green needle-shaped crystal of **7**, and a red-brown, needle-shaped crystal of **9** were measured on an AED II (Siemens) diffractometer. The data for a black, needle-shaped crystal of **8** were measured on a Syntex R3 diffractometer. Crystal parameters and additional details of the data collection and reduction are given in Table I. Lattice parameters for all compounds were obtained from a least-squares fit to the setting angles of 25 reflections with $7 \leq 2\vartheta \leq 27°$. Empirical absorption corrections (ψ-scans) were carried out in each case (6 reflections; $3.5 \leq 2\vartheta \leq 36°$). All structures were solved by standard Patterson and difference Fourier methods and refined[26] with anisotropic thermal parameters for all non-hydrogen atoms unless stated otherwise below. Neutral atom scattering factors and anomalous dispersion corrections for non-hydrogen atoms were taken from ref 24 and hydrogen atom scattering factors from ref 25. All methylene hydrogen atoms were placed at calculated positions with d(C–H) = 0.96 Å, while the methyl

(22) Gritzner, G.; Kuta, J. *Pure Appl. Chem.* **1982**, *54*, 1527–1532.
(23) (a) Carlin, R. L. In *Magnetochemistry*; Springer-Verlag: New York, 1986; p 3. (b) O'Connor, C. J. *Progr. Inorg. Chem.* **1979**, *29*, 205–283.
(24) *International Tables of Crystallography*; Kynoch: Birmingham, England, 1974; Vol. IV, pp 99 and 149.
(25) Stewart, R. F.; Davidson, E. R.; Simpson, W. T. *J. Chem. Phys.* **1965**, *42*, 3175–3187.
(26) All calculations were carried out on an ECLIPSE computer with the SHELXTL program package (Nicolet 1987).

Table II. Atom Coordinates ($\times 10^4$) of the Cation $[L'Mn(\mu\text{-}CH_3CO_2)_3MnL']^+$ in $[L'_2Mn_2(CH_3CO_2)_3][BPh_4]$

atom	x	y	z	U_{equiv}
Mn1	1996 (1)	3491 (1)	4452.0 (4)	0.0458 (8)
Mn2	1968 (1)	8550 (1)	9333.8 (4)	0.0546 (8)
O1	1580 (5)	7518 (6)	10250 (2)	0.081 (4)
O2	1344 (5)	9403 (5)	10298 (2)	0.069 (4)
O3	3065 (1)	8605 (6)	10254 (2)	0.084 (4)
O4	1415 (5)	7590 (5)	9593 (2)	0.073 (4)
O5	3040 (5)	8419 (6)	9596 (2)	0.094 (4)
O6	1505 (5)	9486 (5)	9641 (2)	0.077 (4)
C21	1462 (6)	7244 (6)	9918 (3)	0.046 (4)
C22	1338 (7)	6377 (6)	9909 (4)	0.078 (4)
C23	1328 (6)	9738 (6)	9980 (4)	0.051 (4)
C24	1012 (8)	10539 (7)	9983 (5)	0.103 (5)
C25	3341 (6)	8507 (8)	9931 (3)	0.063 (4)
C26	4232 (8)	8372 (10)	9926 (5)	0.141 (7)
N1	2630 (6)	7687 (6)	11011 (3)	0.063 (5)
N2	2391 (6)	9319 (6)	11049 (3)	0.062 (5)
N3	1080 (6)	8331 (7)	11058 (2)	0.074 (5)
N4	971 (7)	8656 (7)	8848 (3)	0.092 (6)
N5	2474 (6)	9399 (6)	8858 (3)	0.067 (5)
N6	2392 (7)	7758 (7)	8803 (3)	0.087 (6)
C1	3209 (9)	8207 (9)	11202 (5)	0.116 (7)
C2	2961 (8)	8926 (8)	11324 (3)	0.066 (4)
C3	1706 (8)	9532 (8)	11263 (4)	0.088 (5)
C4	1199 (9)	8929 (9)	11356 (4)	0.104 (6)
C5	1287 (8)	7554 (8)	11233 (4)	0.074 (5)
C6	2083 (10)	7390 (10)	11291 (4)	0.126 (7)
C7	3064 (9)	7080 (7)	10798 (4)	0.080 (5)
C8	2753 (8)	9994 (7)	10875 (4)	0.089 (5)
C9	328 (8)	8263 (9)	10881 (4)	0.089 (5)
C11	1180 (9)	9326 (10)	8571 (4)	0.110 (6)
C12	1812 (9)	9766 (9)	8687 (4)	0.108 (6)
C13	2938 (10)	8984 (9)	8562 (4)	0.102 (6)
C14	2971 (10)	8192 (10)	8605 (5)	0.122 (7)
C15	1762 (9)	7647 (10)	8527 (4)	0.118 (7)
C16	1034 (9)	7924 (9)	8624 (4)	0.108 (6)
C17	222 (8)	8732 (10)	9048 (4)	0.122 (7)
C18	2942 (8)	9984 (7)	9067 (4)	0.077 (5)
C19	2710 (9)	7065 (9)	8959 (4)	0.110 (6)

groups were treated as rigid bodies, each with three rotational variables. The function minimized during refinement was $\sum w(|F_o| - |F_c|)^2$, where $w = 1/\sigma^2(I)$.

Some special features of the structure determinations are now following.

$[L'_2Mn_2(\mu\text{-}CH_3CO_2)_3][BPh_4]$ (4). The crystals finally obtained after several attempts of recrystallization and slow growth of crystals were still of low X-ray quality. The crystal selected did not diffract above $2\vartheta = 26°$, and, therefore, the ratio of observed unique reflections to least-squares parameters is rather low (8.03). In order to keep the number of variables reasonably small the carbon and boron atoms of the BPh_4 anion and of the cyclic amine ligand were only refined with isotropic thermal parameters, whereas the $Mn_2N_6O_6$-core of the cation in **4** was refined with use of anisotropic thermal parameters. Table II summarizes the final atom parameters.

$[L_2Mn_2(OH)_2(\mu\text{-}O)_2][Mn_3(C_2O_4)_4(H_2O)_2]\cdot 6H_2O$ (7). The protons bound to the terminal OH groups of the anion in **7** and the water molecules of crystallization were not located and were not included in the refinement. See the results section for structural and chemical arguments for the assignment of these protons in the formula given above. Atom parameters are given in Table III.

$[L_4Mn_4O_6]Br_4\cdot 5.5H_2O$ (8). In **8** a disorder of one bromide anion is observed. When the occupancy factor of Br5 was treated as a variable during refinement cycles a value of 0.49 was obtained which was set to 0.5 in the final cycle. The final discrepancy factor R increased significantly if the scattering factors of an oxygen atom with an occupancy of 1.0 was introduced at the position of Br5 instead. This had been done erroneously in the previously published structure determination.[13] The final atom parameters are given in Table IV.

Results and Discussion

Synthesis. In previous work,[7] it was shown that spontaneous self-assembly of binuclear manganese(III) complexes from manganese(III) acetate, sodium acetate, and the respective cyclic triamine 1,4,7-triazacyclononane (L) and *N,N',N''*-trimethyl-1,4,7-triazacyclononane (L') in an ethanol mixture (85 vol %)

Table III. Atom Coordinates ($\times 10^4$) of $[L_2Mn_2(\mu\text{-}O)_2(OH)_2][Mn_3(C_2O_4)_4(OH_2)_2]\cdot 6H_2O$

atom	x	y	z
Mn1	327.1 (8)	9503.2 (6)	561.5 (5)
O1	854 (3)	10399 (3)	265 (2)
O2	−296 (4)	10031 (3)	1176 (2)
N1	1025 (4)	8775 (3)	−8 (3)
N2	1710 (4)	9258 (3)	1410 (3)
N3	−132 (5)	8399 (4)	848 (3)
C1	2142 (6)	8604 (6)	414 (4)
C2	2553 (6)	9092 (5)	1081 (4)
C3	1536 (7)	8576 (6)	1855 (4)
C4	462 (7)	8314 (6)	1658 (4)
C5	165 (7)	7741 (5)	373 (4)
C6	356 (7)	8028 (5)	−214 (4)
Mn2	3949.7 (8)	10515.8 (7)	3533.5 (5)
O3	4619 (4)	11303 (3)	2926 (3)
C7	5000	10974 (6)	2500
C8	5000	10028 (6)	2500
O4	4594 (4)	9674 (3)	2914 (2)
O5	5416 (4)	10719 (3)	4490 (3)
O6	3856 (4)	9622 (3)	4338 (2)
O7	2988 (3)	11380 (3)	3854 (2)
O8	2387 (4)	10422 (3)	2649 (2)
O9	1418 (3)	11995 (3)	3454 (2)
O10	904 (3)	11154 (3)	2185 (2)
C9	4549 (5)	9683 (4)	4956 (4)
C10	2080 (5)	11500 (4)	3392 (3)
C11	1767 (5)	10974 (4)	2673 (4)
Mn3	0	2127.3 (9)	2500
O11	655 (4)	13026 (3)	1956 (3)
O_w1	1882 (6)	9000 (4)	3796 (4)
O_w2	2320 (5)	2620 (5)	1533 (4)
O_w3	2659 (5)	1346 (5)	730 (5)

results in the formation of **1** and **2**, which were isolated as deep red PF_6, BPh_4, or ClO_4 salts. These compounds may be recrystallized from acetonitrile; aqueous solutions of **1** and **2** are unstable with respect to disproportionation as we will show here. When

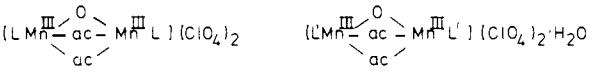

1 2

manganese(II) perchlorate hexahydrate dissolved in anhydrous methanol with *N,N',N''*-trimethyl-1,4,7-triazacyclononane under an argon atmosphere were used as starting materials, and solid sodium perchlorate was added, colorless crystals of $[L'_2Mn^{II}_2(\mu\text{-}OH)(\mu\text{-}CH_3CO_2)_2](ClO_4)$ (**3**) precipitated.[9] The presence of the hydroxo bridge was clearly demonstrated by a sharp band at 3520 cm^{-1} in the infrared (ν(OH)). The analogous reaction of manganese(II) acetate tetrahydrate, on the other hand, in methanol yielded after addition of sodium tetraphenylborate colorless microcrystals of a different manganese(II) dimer $[L'Mn^{II}(\mu\text{-}CH_3CO_2)_3Mn^{II}L'][BPh_4]$ (**4**), which was recrystallized from hot acetonitrile affording single crystals suitable for X-ray crystallography. Both **3** and **4** decompose in aqueous solution; they are air sensitive in solution and moderately so in the solid state.

3 4

While the manganese(III) dimers **1** and **2** are perfectly stable in aprotic solvents such as acetonitrile, we have now found that in acidic aqueous solutions they undergo fast disproportionation and dissociation reactions. A variety of compounds were isolated from such mixtures, the composition of which depended on the nature of the counteranions added. Thus neutral aqueous solutions of **1** changed color from red to green within minutes under anaerobic conditions, and addition of solid $Na[BPh_4]$ initiated the precipitation of the mixed-valent manganese(III/IV) dimer $[LMn^{III}(\mu\text{-}O)_2(\mu\text{-}CH_3CO_2)Mn^{IV}L][BPh_4]_2CH_3CN$ (**5**) (after recrystallization from hot acetonitrile), which has been charac-

Table IV. Atom Coordinates ($\times 10^4$) of $[L_4Mn_4O_6]Br_4 \cdot 5.5H_2O$

atom	x	y	z
Br1	5000	0000	0000[a]
Br2	5441.1 (8)	4328 (1)	1589.4 (6)
Br3	8205.6 (7)	4228.7 (9)	1280.6 (5)
Br4	2227.2 (7)	8065 (1)	2170.2 (7)
Br5	1769 (2)	789 (3)	-8 (2)[a]
Mn1	5957.1 (8)	7847 (1)	1724.1 (7)
Mn2	4619.4 (8)	9344 (1)	1988.7 (7)
Mn3	4115.3 (8)	7373 (1)	1077.8 (7)
Mn4	4846.0 (8)	7097 (1)	2607.8 (7)
O1	5575 (3)	9082 (4)	1863 (3)
O2	5152 (3)	7406 (5)	1090 (3)
O3	5767 (3)	7172 (5)	2392 (3)
O4	4201 (4)	6752 (5)	1836 (3)
O5	4020 (3)	8675 (5)	1306 (3)
O6	4613 (4)	8427 (5)	2605 (3)
N1	6448 (5)	8501 (6)	1032 (4)
N2	7073 (4)	8246 (6)	2306 (4)
N3	6618 (4)	6603 (6)	1550 (4)
N4	4560 (4)	10631 (6)	1418 (4)
N5	5132 (5)	10402 (6)	2696 (4)
N6	3589 (4)	9992 (6)	2130 (4)
N7	3828 (4)	7858 (6)	119 (3)
N8	3992 (5)	5960 (6)	619 (4)
N9	2887 (4)	7205 (6)	851 (4)
N10	5472 (5)	7235 (6)	3578 (4)
N11	5079 (4)	5583 (6)	2834 (4)
N12	3933 (4)	6786 (6)	3033 (4)
C1	7025 (7)	9298 (10)	1338 (6)
C2	7496 (8)	8964 (10)	1973 (6)
C3	7510 (7)	7299 (9)	2524 (7)
C4	7394 (7)	6532 (9)	2015 (6)
C5	6686 (8)	6678 (9)	879 (5)
C6	6786 (8)	7732 (9)	676 (6)
C11	5068 (8)	11444 (9)	1748 (6)
C12	5491 (8)	11195 (10)	2400 (6)
C13	4538 (7)	10780 (12)	3032 (6)
C14	3749 (6)	10338 (10)	2791 (5)
C15	3262 (7)	10798 (9)	1632 (5)
C16	3740 (7)	10952 (10)	1177 (6)
C21	3943 (8)	7045 (9)	-313 (5)
C22	4177 (9)	6062 (9)	-4 (6)
C23	3226 (7)	5494 (9)	554 (7)
C24	2709 (7)	6113 (10)	808 (7)
C25	2488 (7)	7760 (12)	256 (6)
C26	3013 (6)	8254 (10)	-65 (6)
C31	5914 (7)	6338 (9)	3807 (6)
C32	5806 (8)	5517 (11)	3362 (6)
C33	4395 (8)	5062 (9)	2975 (8)
C34	3733 (7)	5704 (9)	2957 (7)
C35	4132 (8)	7160 (12)	3719 (6)
C36	4911 (8)	7557 (12)	3943 (6)
O_w1	9129 (4)	7727 (6)	1042 (4)
O_w2	2325 (6)	2949 (9)	504 (5)
O_w3	8768 (6)	5779 (9)	299 (5)
O_w4	3515 (7)	3496 (9)	1576 (6)
O_w5	738 (7)	7753 (10)	825 (6)
O_w6	377 (11)	5651 (16)	298 (9)[a]

[a] Site occupancy 0.5; all other atoms 1.0.

terized by X-ray crystallography.[10] In the previous communication[10] oxygen had been invoked as necessary oxidant, which in fact is not. **2** also disproportionates under anaerobic conditions in 1 M perchloric acid to give another mixed valent dimer $[L'Mn^{III}(\mu\text{-}O)(\mu\text{-}CH_3CO_2)_2Mn^{IV}L'](ClO_4)_3$ (**6**), which has also been characterized by X-ray crystallography.[9] Again oxygen is not a necessary oxidant; **2** disproportionates under anaerobic conditions. In both disproportionation reactions manganese(II) is also produced. This was nicely demonstrated when an aqueous

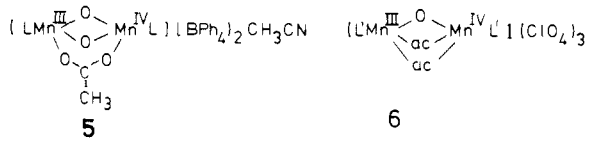

5 **6**

solution of sodium oxalate was allowed to slowly diffuse within

Scheme I

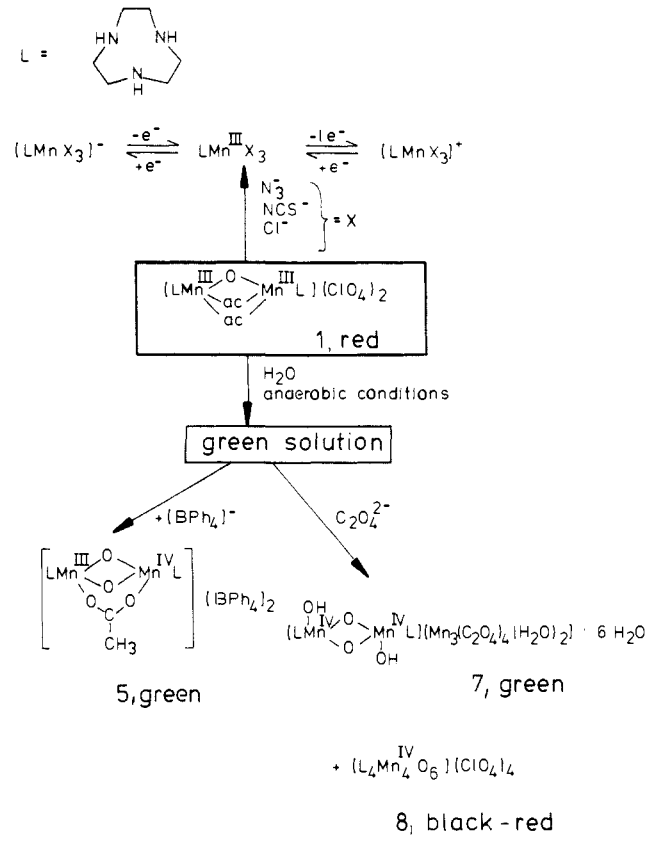

24 h under anaerobic conditions into an aqueous solution of **1**. Beautiful green crystals of $[L_2Mn^{IV}_2(OH)_2(\mu\text{-}O)_2][Mn^{II}_3(C_2O_4)_4(H_2O)_2] \cdot 6H_2O$ (**7**) of X-ray quality precipitated.

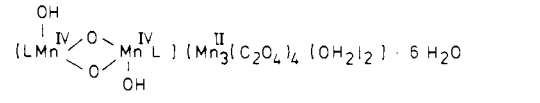

7

The cation is a Mn^{IV}_2 dimer and the anion is a polymer composed of octahedrally coordinated manganese(II) centers (see below). Black-red crystals of the tetramer $[L_4Mn^{IV}_4(\mu\text{-}O)_6](ClO_4)_4$ (**8**) also formed as a byproduct. When an aqueous solution of **1** was added under anaerobic conditions to an aqueous solution of sodium oxalate, green microcrystals of **7** precipitated immediately as the sole product. These experiments clearly show that **1** is unstable in aqueous solution toward disproportionation, i.e., Mn^{IV} and Mn^{II} are produced, and dissociation of the μ-acetato bridges occurs. Scheme I summarizes the reactions of **1** investigated in this study.

The tetramer **8** has been briefly described previously.[13] It is readily formed in an alkaline aqueous solution containing manganese(II) and 1,4,7-triazacyclononane in the presence of oxygen. It is also the thermodynamically most stable species in aqueous solutions containing Mn(III) and the cyclic amine L. Thus in the absence of any further counteranions which would initiate the precipitation of other binuclear intermediates **1** slowly disproportionates forming **8** and Mn(II).

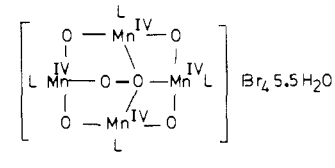

8

Interestingly, such a tetramer is not generated if the *N*-methylated ligand *N,N',N''*-trimethyl-1,4,7-triazacyclononane (L')

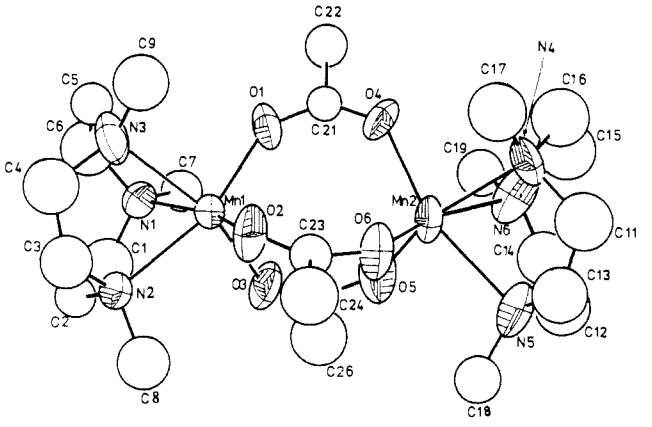

Figure 1. Structure of the $[L'_2Mn_2(\mu\text{-}CH_3CO_2)_3]^+$ cation in **4**, showing 40% probability thermal ellipsoids and the atom labeling scheme (open circles represent atoms with an isotropic thermal parameter).

Scheme II

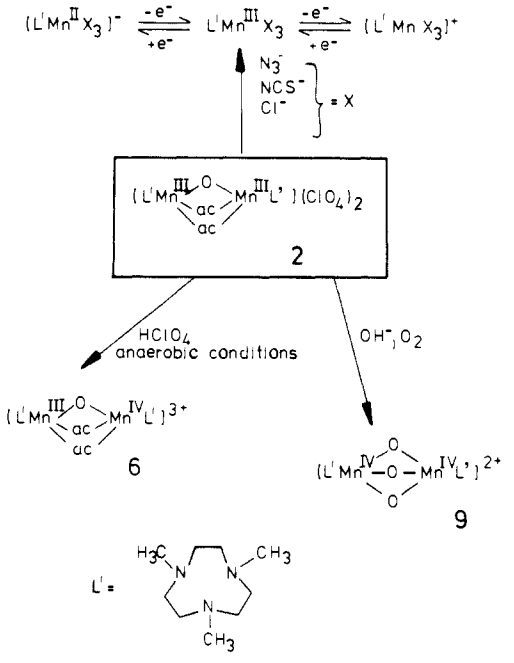

is used instead of L. Thus **2** disproportionates under anaerobic conditions in acid aqueous solution to yield **6** as the only isolable product, but in alkaline solution in the presence of oxygen the novel dimer $[L'Mn^{IV}(\mu\text{-}O)_3Mn^{IV}L']^{2+}$ (**9**) formed which was isolated as red hexafluorophosphate salt. Traces of MnO_2 were also generated. Scheme II summarizes the reactions of **2** investigated in this study.

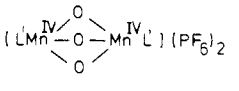

9

The inherent lability of the μ-acetato *and* the oxo-bridges in **1** and **2** was demonstrated by the reaction of **1** and **2** dissolved in acetonitrile with concentrated hydrochloric acid. Red-brown microcrystals of $LMnCl_3$ or $L'MnCl_3$ precipitated immediately. From ethanolic solutions of **1** or **2**, crystals of $LMn(NCS)_3$ or $L'Mn(NCS)_3$ formed upon addition of NaSCN. The corresponding tris-azido complexes have been described previously,[12] including the X-ray structure of $LMn(N_3)_3$.

Description of Structures. $[L'_2Mn^{II}_2(\mu\text{-}CH_3CO_2)_3][BPh_4]$ (4). Figure 1 shows the cation $[L'_2Mn^{II}_2(\mu\text{-}CH_3CO_2)_3]^+$ and the atom labeling scheme; Table VI summarizes important bond lengths and angles. Each manganese atom has a distorted octahedral coordination sphere comprised of three symmetrically bridging carboxylates and a facially coordinating tridentate amine ligand. The largest deviation from idealized 90° interbond angles is −14.1° and +14.5°, which occur within the five-membered N–Mn–N chelate ring and between two oxygen atoms of two carboxylates, respectively. The Mn–N bond lengths are quite large (average 2.35 (1) Å). The Mn–O distance is 2.12 (1) Å and is only slightly shorter than the sum of the effective ionic radii of high-spin Mn(II) (coordination number 6) and O^{2-} (2.17 Å).[27] The Mn1···Mn2 distance is 4.034 (2) Å and is most probably longer than in the hydroxo-bridged species $[L'_2Mn^{II}_2(\mu\text{-}OH)(\mu\text{-}CH_3CO_2)_2]^+$ for which a Mn···Mn distance of 3.5 ± 0.2 Å is estimated from a comparison with the analogous iron(II) dimer.[28]

The C–N bond lengths found in the cyclic amine ligand are normal (range 1.44–1.51 (2) Å), and the C–C bond lengths are

Table V. Atom Coordinates (×10⁴) of $[L_2Mn_2(\mu\text{-}O)_3](PF_6)_2\cdot H_2O$

atom	*x*	*y*	*z*
Mn1	718 (2)	2500	5633 (1)
Mn2	−531 (2)	2500	4633 (1)
O1	−1094 (7)	2500	5531 (4)
O2	670 (6)	3264 (3)	4937 (3)
N1	2803 (9)	2500	5751 (6)
N2	785 (8)	3363 (4)	6454 (4)
N3	77 (12)	2500	3582 (6)
N4	−1937 (8)	1634 (5)	4269 (4)
C1	−3204 (11)	2104 (6)	4187 (8)
C2	−2115 (12)	924 (7)	4750 (6)
C3	−1473 (16)	1333 (7)	3603 (7)
C4	3435 (15)	2500	5062 (8)
C5	−143 (12)	4049 (6)	6344 (5)
C6	433 (15)	2915 (5)	7089 (5)
C7	1572 (14)	2500	3538 (8)
C8	3126 (11)	1755 (7)	6138 (7)
C9	2152 (10)	3686 (8)	6471 (7)
C10	−391 (15)	1687 (11)	3318 (8)
P1	1052 (3)	5229 (2)	8499 (2)
F11	846 (9)	6163 (4)	8418 (4)
F12	1264 (8)	4279 (5)	8562 (5)
F13	2368 (8)	5326 (5)	8879 (4)
F14	311 (11)	5220 (8)	9142 (4)
F15	−242 (8)	5104 (7)	8112 (6)
F16	1774 (10)	5222 (6)	7825 (4)
O_w	1591 (15)	2500	8669 (8)

Table VI. Selected Bond Distances (Å) and Angles (deg) of the Cation in $[L'_2Mn_2(\mu\text{-}CH_3CO_2)_3][BPh_4]$

Mn1–O1	2.099 (9)	Mn2–O4	2.122 (9)
Mn1–O2	2.128 (8)	Mn2–O5	2.070 (9)
Mn1–O3	2.107 (8)	Mn2–O6	2.094 (9)
Mn1–N1	2.36 (1)	Mn2–N4	2.37 (1)
Mn1–N2	2.31 (1)	Mn2–N5	2.34 (1)
Mn1–N3	2.34 (1)	Mn2–N6	2.36 (1)
O1–Mn1–O2	104.1 (3)	O4–Mn2–O5	98.5 (4)
O1–Mn1–O3	99.3 (3)	O4–Mn2–O6	104.5 (3)
O1–Mn1–N1	89.0 (3)	O4–Mn2–N4	90.4 (4)
O1–Mn1–N2	162.0 (3)	O4–Mn2–N5	161.5 (3)
O1–Mn1–N3	90.6 (4)	O4–Mn2–N6	88.7 (4)
O2–Mn1–O3	102.5 (3)	O5–Mn2–O6	103.1 (3)
O2–Mn1–N1	162.1 (3)	O5–Mn2–N4	162.1 (3)
O2–Mn1–N2	88.0 (3)	O5–Mn2–N5	90.9 (4)
O2–Mn1–N3	90.6 (3)	O5–Mn2–N6	88.2 (4)
O3–Mn1–N1	87.0 (3)	O6–Mn2–N4	89.4 (4)
O3–Mn1–N2	90.7 (3)	O6–Mn2–N5	88.6 (3)
O3–Mn1–N3	161.0 (3)	O6–Mn2–N6	160.9 (4)
N1–Mn1–N2	76.6 (4)	N4–Mn2–N5	76.5 (4)
N1–Mn1–N3	76.9 (3)	N4–Mn2–N6	76.5 (4)
N2–Mn1–N3	75.9 (4)	N5–Mn2–N6	75.7 (4)

(27) Shannon, R. D. *Acta Crystallogr.* **1976**, *A32*, 751–767.
(28) (a) Chaudhuri, P.; Wieghardt, K.; Nuber, B.; Weiss, J. *Angew. Chem., Int. Ed. Engl.* **1985**, *24*, 778–779. (b) Hartmann, J. R.; Rardin, R. L.; Chaudhuri, P.; Pohl, K.; Wieghardt, K.; Nuber, B.; Weiss, J.; Papaefthymiou, G. C.; Frankel, R. B.; Lippard, S. J. *J. Am. Chem. Soc.* **1987**, *109*, 7387–7396.

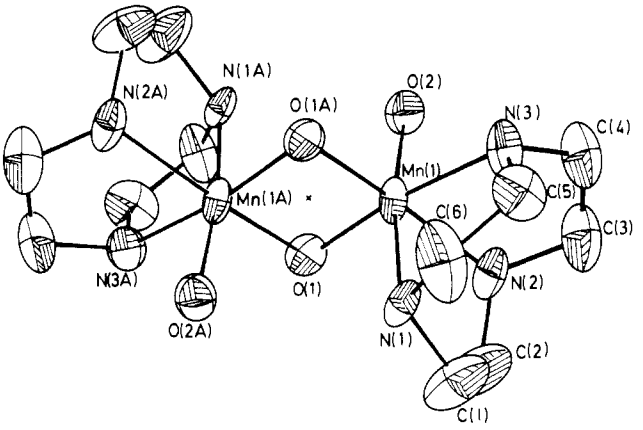

Figure 2. Structure of the $[L_2Mn_2(OH)_2(\mu\text{-}O)_2]^{2+}$ cation in **7**, showing 40% probability thermal ellipsoids and the atom labeling scheme (× denotes a crystallographic center of symmetry).

Table VII. Selected Bond Distances (Å) and Angles (deg) of $[L_2Mn_2(\mu\text{-}O)_2(OH)_2][Mn_3(C_2O_4)_4(OH_2)_2]\cdot 6H_2O$

Mn1–O1	1.818 (5)	Mn2–O3	2.136 (6)
Mn1–O2	1.881 (5)	Mn2–O4	2.195 (5)
Mn1–O1′	1.834 (3)	Mn2–O5	2.219 (4)
Mn1–N1	2.058 (6)	Mn2–O6	2.180 (5)
Mn1–N2	2.055 (5)	Mn2–O7	2.152 (5)
Mn1–N3	2.064 (6)	Mn2–O8	2.213 (4)
Mn1···Mn1′	2.625 (2)	Mn3–O9	2.162 (4)
		Mn3–O10	2.221 (5)
		Mn3–O11	2.171 (6)
Mn1–O1–Mn1′	91.9 (2)		
O2–Mn1–O1	97.0 (2)	O3–Mn2–O4	77.1 (2)
N1–Mn1–O1	90.9 (2)	O3–Mn2–O5	87.2 (2)
N2–Mn1–O1	94.1 (2)	O3–Mn2–O6	160.2 (2)
N3–Mn1–O1	172.3 (2)	O3–Mn2–O7	98.7 (2)
O1′–Mn1–O1	88.1 (2)	O3–Mn2–O8	94.5 (2)
N1–Mn2–O2	171.2 (2)	O4–Mn2–O5	98.6 (2)
N2–Mn2–O2	93.5 (2)	O4–Mn2–O6	94.9 (2)
N3–Mn2–O2	90.4 (2)	O4–Mn2–O7	164.4 (1)
O1′–Mn2–O2	94.1 (2)	O4–Mn2–O8	88.8 (2)
N2–Mn2–N1	82.0 (2)	O5–Mn2–O6	76.0 (2)
N3–Mn2–N1	81.6 (3)	O5–Mn2–O7	96.1 (2)
O1′–Mn2–N1	90.0 (2)	O5–Mn2–O8	172.6 (2)
N3–Mn2–N2	83.1 (2)	O6–Mn2–O7	93.6 (2)
O1′–Mn2–N2	171.7 (2)	O6–Mn2–O8	103.6 (2)
N3–Mn2–O1′	93.7 (2)	O7–Mn2–O8	76.6 (2)
O9–Mn3–O9	168.4 (3)		
O10–Mn3–O9	76.0 (2)		
O10′–Mn3–O9	95.5 (2)		
O11–Mn3–O9	95.7 (2)		
O11′–Mn3–O9	92.3 (2)		
O10′–Mn3–O9′	75.9 (2)		
O10′–Mn3–O10	86.9 (3)		
O10–Mn3–O11	91.1 (2)		
O10–Mn3–O11′	167.8 (2)		
O11–Mn3–O11′	93.4 (3)		

short (range 1.39–1.43 (2) Å) compared to the normal value of 1.54 Å. Such short C–C distances are often observed in crown complexes, primarily due to uncorrected thermal motion. These observations are also made for structures **7**, **8**, and **9** (see below) and will not be further discussed in detail there.

$[L_2Mn^{IV}_2(\mu\text{-}O)_2(OH)_2][Mn^{II}_3(C_2O_4)_4(OH_2)_2]\cdot 6H_2O$ (7). The structure of **7** is quite complex as it consists of a dimeric cation and a polymeric anion $\{[Mn^{II}_3(C_2O_4)_4(OH_2)_2]^{2-}\}_\infty$. Let us consider the cation first, which is shown in Figure 2; relevant bond distances and angles are summarized in Table VII. The dication consists of a planar bis(μ-oxo)dimanganese(IV) core with a capping 1,4,7-triazacyclononane ligand coordinated to each manganese center. The distorted octahedral environment of each Mn center is completed by a terminal hydroxo group. The cation possesses a crystallographically imposed center of symmetry and, therefore, the two coordinated OH groups are in anti-position with respect

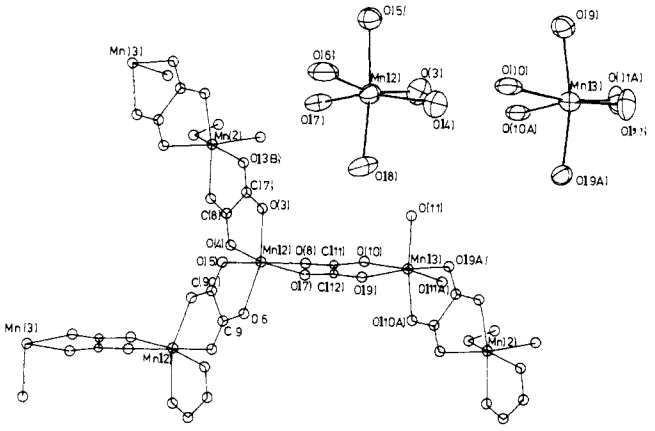

Figure 3. Schematic view of the connectivity in the polymeric $[Mn_3(C_2O_4)_4(OH_2)_2]^{-2}$ anion in **7** and the structures of the MnO_6 octahedra of Mn2 and Mn3 showing 40% probability thermal ellipsoids and the atom labeling scheme.

to each other. The average Mn–N bond distance in **7** is 2.059 (5) Å, which is shorter by 0.058 Å than the corresponding value found in the mixed-valent $Mn^{III}Mn^{IV}$ species **5**, and it is shorter by 0.12 Å compared with the manganese(III) dimer **1**. Thus the Mn–N distances clearly respond to the removal of one electron from an antibonding e_g*-orbital on going from Mn(III) (d^4 high spin) to Mn(IV) (d^3). The dimensions of the $\{Mn^{IV}_2O_2\}^{4+}$ core compare well with those in $[(phen)_4Mn^{IV}_2(\mu\text{-}O)_2](ClO_4)_4\cdot CH_3CN$,[29] and in the mixed-valent complex $[(bispicen)_2Mn_2O_4]^{3+}$,[30] the average Mn^{IV}–O_{oxo} bond length is 1.826 (4) Å. The Mn^{IV}–OH bond is significantly longer (1.881 (5) Å).

The proton of the terminal OH group has not been located in the present structure analysis. Therefore, in principle, a coordinated water molecule or even a terminal oxo group are conceivable, which would change the overall charge of the dication from 2+ (hydroxo groups) to 4+ (aqua ligands) or zero (oxo groups). The latter alternative is readily ruled out, since a terminal Mn^{IV}=O bond distance is expected to be shorter than the bonds in Mn–O–Mn.[31] Furthermore, **7** would be composed of a neutral dimer and a neutral polymer—a highly unlikely situation. A Mn^{IV}–OH_2 moiety has not been characterized by X-ray crystallography to date; in fact, no complex of Mn^{IV} is known to have a coordinated H_2O molecule. Furthermore, the protons of a Mn^{IV}–OH_2 group would be highly acidic and **7** has been prepared at pH 8–10. Thus we feel confident that the data at hand are sufficient to demonstrate the presence of two OH groups in the cation of **7** and that the manganese centers are in the oxidation state +IV.

The anion in **7**, $\{[Mn^{II}_3(C_2O_4)_4(H_2O)_2]^{2-}\}_\infty$, is a polymer forming a net-shaped layer with large cavities into which the dications are positioned. It is composed of two differently coordinated manganese(II) centers (Figure 3). Mn2 coordinates to three oxalato ligands in a bidentate fashion generating a slightly distorted octahedral environment around Mn2. Mn3, in contrast, is coordinated to only two $C_2O_4^{2-}$ ligands (bidentate) and to two cis-positioned H_2O molecules; Mn3 is also in distorted octahedral environment ($Mn^{II}O_6$ octahedron). The ratio Mn2 to Mn3 is 2:1. The $C_2O_4^{2-}$ ligands are tetradentate; they link Mn3 centers with other Mn3 centers and Mn2 forming a net-shaped layered structure (Figure 4). The Mn–$O_{oxalate}$ bond distances in Mn2 and Mn3 (average 2.187 Å) are very similar to those in $K_2Mn^{II}(C_2O_4)_2\cdot 2H_2O$;[32] they are significantly longer than those in $K_3[Mn^{III}(C_2O_4)_3]\cdot 3H_2O$,[33] and they correspond to the sum of the

(29) Stebler, M.; Ludi, A.; Bürgi, H.-B. *Inorg. Chem.* **1986**, *25*, 4743–4750.
(30) Collins, M. A.; Hogson, D. J.; Michelsen, K.; Towle, D. K. *J. Chem. Soc., Chem. Commun.* **1987**, 1659–1661.
(31) A highly reactive Mn^{IV}=O porphyrine species has recently been described in tetrahydrofurane solution at −70 °C: Schappacher, M.; Weiss, R. *Inorg. Chem.* **1987**, *26*, 1189–1190.
(32) Schulz, H. *Acta Crystallogr.* **1974**, *B30*, 1318–1332.

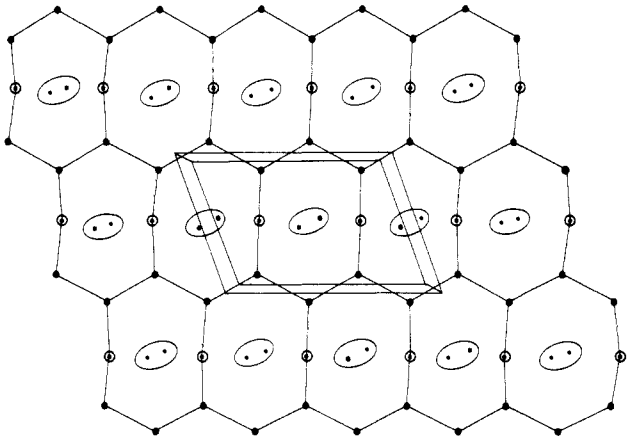

Figure 4. Schematic representation of the layered structure of **7** with one unit cell (●, Mn2; ⊙, Mn3; ⬭, dimeric cation in **7**; each line between an Mn2 and Mn3 center represents a tetradentate oxalate ligand).

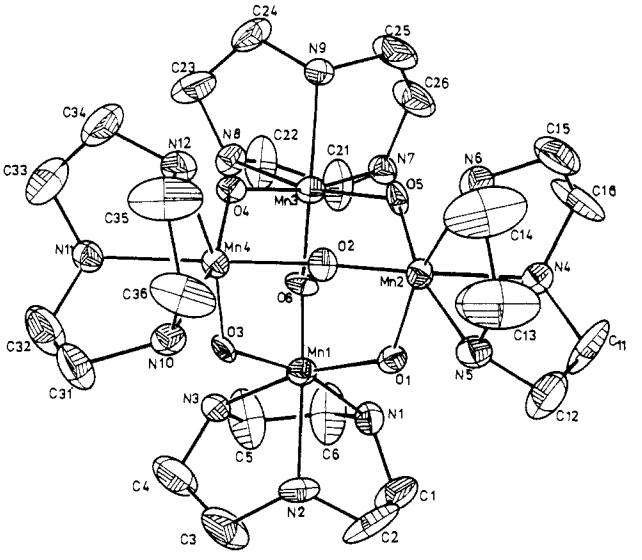

Figure 5. Structure of the $[L_4Mn_4O_6]^{4+}$ cation in **8**, showing 40% probability thermal ellipsoids and the atom labeling scheme.

effective ionic radii of octahedrally coordinated, high-spin Mn(II) and O^{2-} (2.17 Å). Thus, there is no doubt that the manganese centers of the anion in **7** are in the oxidation state +II (Mn^{II}, d^5 high spin).

The conceivable proton ambiguity at Mn3–(OH_2) is only a formal one. Since the protons of the coordinated H_2O molecules of Mn3 have again not been located, a Mn3–OH group would be an alternative formulation yielding a 4-charged anion. But octahedral complexes of Mn(II) containing a terminal OH ligand in aqueous solution are not known; $[Mn(OH_2)_6]^{2+}$ is not a very effective Brønstedt acid. The Mn–OH_2 bond distance of 2.171 (6) Å agrees well with those found in many aqua complexes of Mn(II).[34] Thus the data obtained by X-ray crystallography and the magnetic susceptibility data (see below) lead to an unambiguous assignment of oxidation states of the manganese centers as well as the location of the protons in **7**.

$[L_4Mn^{IV}_4O_6]Br_4 \cdot 5.5H_2O$ (8). The structure of **8** has been briefly described previously, where it has been formulated as "$[L_4Mn_4O_6]Br_{3.5}OH_{0.5} \cdot 5H_2O$".[13] The present reinvestigation of this structure using a better single crystal and a new X-ray data set has shown that a disorder phenomenon of one bromide anion (Br5) has been previously incorrectly taken into consideration. Thus the correct formulation of this black red material is as shown in the title. Table VIII summarizes bond lengths and angles in **8**.

Crystals of **8** consist of the tetranuclear cation $[L_4Mn_4O_6]^{4+}$ (Figure 5), uncoordinated bromide ions, and water molecules of crystallization. The four Mn centers occupy the corners of an idealized tetrahedron, and one oxo-bridging group is located above the center of each of the six edges. The $\{Mn_4O_6\}^{4+}$ moiety corresponds to an adamantane skeleton. Each Mn^{IV} ion is in a distorted octahedral environment comprised of three facially coordinated amine nitrogen atoms and three oxygen atoms. The average Mn–N bond distance of 2.086 Å is only slightly larger than those found in the cation of **7** and is indicative of the presence of manganese(IV) centers in **8**. The average Mn–O bond length is 1.797 Å, typical for Mn–O–Mn entities. The average Mn···Mn

Table VIII. Bond Distances (Å) and Angles (deg)[a] in $[L_4Mn_4O_6]Br_4 \cdot 5.5H_2O$

Mn1–O1	1.809 (6)	Mn2–O1	1.799 (7)
Mn1–O2	1.778 (5)	Mn2–O5	1.785 (6)
Mn1–O3	1.797 (7)	Mn2–O6	1.800 (6)
Mn1–N1	2.098 (9)	Mn2–N4	2.071 (8)
Mn1–N2	2.088 (7)	Mn2–N5	2.085 (8)
Mn1–N3	2.094 (8)	Mn2–N6	2.097 (8)
Mn3–O2	1.812 (6)	Mn4–O3	1.801 (7)
Mn3–O4	1.797 (6)	Mn4–O4	1.800 (6)
Mn3–O5	1.798 (6)	Mn4–O6	1.792 (6)
Mn3–N7	2.090 (7)	Mn4–N10	2.091 (7)
Mn3–N8	2.085 (8)	Mn4–N11	2.059 (8)
Mn3–N9	2.090 (8)	Mn4–N12	2.088 (9)
Mn1···Mn3	3.217 (2)	Mn2···Mn3	3.218 (2)
Mn1···Mn4	3.225 (3)	Mn1···Mn2	3.224 (2)
Mn3···Mn4	3.222 (2)	Mn2···Mn4	3.219 (2)
O2–Mn1–O1	99.5 (3)	Mn1–O1–Mn2	126.6 (3)
O3–Mn1–O1	98.8 (3)	Mn1–O2–Mn3	127.3 (4)
N1–Mn1–O1	89.6 (3)	Mn1–O3–Mn4	127.4 (3)
N2–Mn1–O1	90.3 (3)	Mn3–O4–Mn4	127.2 (4)
N3–Mn1–O1	167.3 (3)	Mn2–O5–Mn3	127.8 (3)
O3–Mn1–O2	100.1 (3)	Mn2–O6–Mn4	127.3 (4)
N1–Mn1–O2	88.9 (3)		
N2–Mn1–O2	165.1 (3)		
N3–Mn1–O2	88.4 (3)		
N1–Mn1–O3	166.5 (3)		
N2–Mn1–O3	89.3 (3)		
N3–Mn1–O3	89.5 (3)		
N2–Mn1–N1	80.0 (3)		
N3–Mn1–N2	80.1 (3)		
N3–Mn1–N1	80.6 (3)		

[a] Bond angles at Mn2, Mn3, and Mn4 are very similar; values are given in Table S10 (supplementary material).

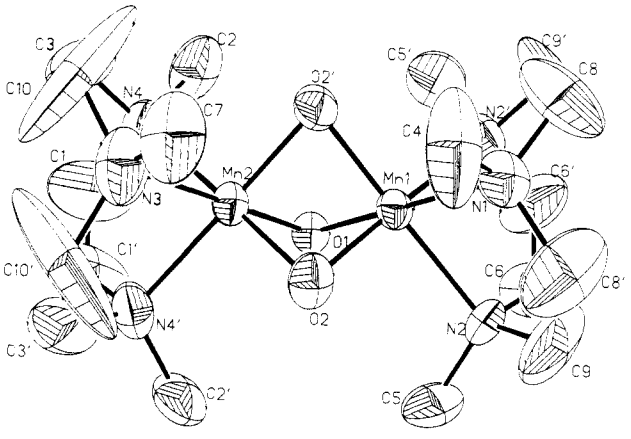

Figure 6. Structure of the $[L'_2Mn_2(\mu\text{-}O)_3]^{2+}$ cation in **9**, showing 40% probability thermal ellipsoids and the atom labeling scheme.

(33) (a) Lis, T.; Matuszewski, J. *Acta Crystallogr.* **1980**, *B36*, 1938–1940. (b) Lis, T.; Matuszewski, J.; Jezowska-Trzebiatowska, B. *Acta Crystallogr.* **1977**, *B33*, 1943–1946. (c) Fackler, J. P., Jr.; Avdeef, A. *Inorg. Chem.* **1974**, *13*, 1864–1875. (d) Avdeef, A.; Costamagna, J. A.; Fackler, J. P., Jr. *Inorg. Chem.* **1974**, *13*, 1854–1863.

(34) (a) Karipides, A.; Reed, A. T. *Inorg. Chem.* **1976**, *15*, 44–47. (b) Bertant, E. F.; Duc, T. Q.; Burlet, P.; Thomas, M.; Moreau, J. M. *Acta Crystallogr.* **1974**, *B30*, 2234–2236. (c) Nakasuka, N.; Azuma, S.; Katayama, C.; Honda, M.; Tanaka, J.; Tanaka, M. *Acta Crystallogr.* **1985**, *C41*, 1176–1179.

Table IX. Bond Distances (Å) and Angles (deg) in $[L'_2Mn_2(\mu\text{-}O)_3](PF_6)_2\cdot H_2O$

Mn1-Mn2	2.296 (2)	Mn2-O1	1.817 (7)
Mn1-O1	1.833 (7)	Mn2-O2	1.821 (6)
Mn1-O2	1.818 (5)	Mn2-N3	2.112 (12)
Mn1-N1	2.109 (9)	Mn2-N4	2.107 (8)
Mn1-N2	2.106 (7)		
Mn1-O1-Mn2	78.0 (3)	O2-Mn1-O1	84.0 (3)
Mn1-O2-Mn2	78.2 (2)	N1-Mn1-O1	180.0 (2)
		N2-Mn1-O1	96.4 (3)
O2-Mn2-O1	84.3 (2)	N1-Mn1-O2	96.1 (3)
N3-Mn2-O1	178.6 (4)	N2-Mn1-O2	96.1 (3)
N4-Mn2-O1	96.1 (3)	O2'-Mn1-O2	85.2 (3)
O2'-Mn2-O2	85.1 (4)	N2'-Mn1-O2	178.7 (3)
N4'-Mn2-O2	96.0 (3)	N2-Mn1-N1	83.5 (3)
N3-Mn2-O2	96.7 (3)	N2-Mn1-N2'	82.6 (4)
N4-Mn2-O2	178.9 (3)		
N4-Mn2-N3	82.9 (3)		
N4'-Mn2-N4	83.0 (4)		

distance in **8** is 3.21 Å. This adamantane-like structural unit has been identified in a number of complexes, e.g., Ti(IV),[35] In(III),[36] Cr(III),[37] and Ta(V).[38] It represents a favorable way to condense four octahedral monomers that contain three labile facially coordinated, unidentate ligands such as water molecules.

$[L'_2Mn^{IV}_2(\mu\text{-}O)_3](PF_6)_2\cdot H_2O$ (9). The complex **9** crystallizes in the orthorhombic space group *Pnma*. Crystals of **9** consist of the dimeric cation $[L'_2Mn^{IV}_2(\mu\text{-}O)_3]^{2+}$, hexafluorophosphate anions, and water molecules of crystallization. Figure 6 shows the structure of **9** and the atom labeling scheme; Table IX gives relevant bond distances and angles. The complex cation possesses a crystallographically imposed mirror plane (atoms Mn1, Mn2, O1, N1, N3 lie on this plane). The site symmetry *m* is not compatible with the symmetry of the cation in **9**, because the three five-membered Mn–N–C–C–N chelate rings of each amine ligand have either ($\lambda\lambda\lambda$) or ($\delta\delta\delta$) conformation and, consequently, the LMn^{IV} moiety does not possess a mirror plane. Therefore, the carbon atoms in **9** are statistically disordered which is born out by unrealistically large anisotropic temperature factors of the C atoms in **9** (Table S9, supplementary material, and Figure 6). The deviation from the site symmetry *m* is not large enough to allow a refinement procedure using a split atom model for these carbon atoms; all attempts to do this have failed. This is a common feature in structure determinations of binuclear species containing these tridentate triazacyclononane ligands.[35]

The Mn^{IV} centers in the cofacial bioctahedral tri-μ-oxo bridged cation are each capped by an *N,N',N''*-trimethyl-1,4,7-triazacyclononane ligand (*fac*-MnN_3O_3 coordination). The average Mn–N distance of 2.108 Å is slightly larger than those found in the cation of **7** with the unalkylated triazacyclononane ligand. Similar increases of M–N bond lengths upon alkylation of secondary amines have been observed previously.[28] The average Mn–O distance is 1.822 Å, which is characteristic of the Mn^{IV}–O–Mn^{IV} entity.

The most interesting facet of this structure is the unprecedented short metal–metal distance of 2.296 (2) Å, which seems to indicate a direct bonding interaction between the two Mn^{IV} centers. This is even more seductive considering the unbridged Mn–Mn distance of 2.93 Å in $Mn_2(CO)_{10}$—a molecule with an undisputed metal–metal bond. Cotton and co-workers have pointed out repeatedly[39] that it is difficult to establish unequivocally the existence of metal–metal bonding in bridged structures.

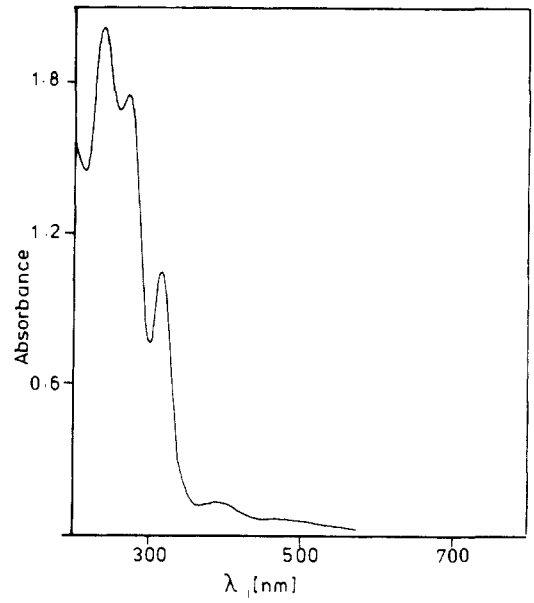

Figure 7. Electronic spectrum of **9** in acetonitrile at 20 °C ([**9**] = 1.1 × 10^{-4} M; *l* = 1.0 cm).

Following the analysis of Cotton and Ucko, and Summerville and Hoffmann,[40] where the M–X–M bonding angle of 70.5° in an ideal cofacial bioctahedron without metal–metal bonding is compared with cases where such an interaction exists ($Mo_2Cl_9^{3-}$ 65°, and $W_2Cl_9^{3-}$ 58°, contrasting $Cr_2Cl_9^{3-}$ with 76°), we come to the conclusion that no Mn^{IV}–Mn^{IV} bond exists in **9** since an Mn–O–Mn angle of 78.1° is found. This angle is quite similar to those in complexes with an $\{M(\mu\text{-}OH)_3M\}^{3+}$ core (M = Co,

(35) (a) Wieghardt, K.; Ventur, D.; Tsay, Y. M.; Krüger, C. *Inorg. Chim. Acta* **1985**, *99*, L25–L27. (b) Babcock, L. M.; Day, V. W.; Klemperer, W. G. *J. Chem. Soc., Chem. Commun.* **1987**, 858–859.

(36) $[L_4In_4(\mu\text{-}OH)_6]^{6+}$: Wieghardt, K.; Kleine-Boymann, M.; Nuber, B.; Weiss, J. *Inorg. Chem.* **1986**, *25*, 1654–1659.

(37) $[(Me_5C_5)_4Cr_4(OH)_6](BF_4)_2$: Wormsbächer, D.; Nicholas, K. M.; Rheingold, A. L. *J. Chem. Soc., Chem. Commun.* **1985**, *721*.

(38) $[F_{12}Ta_4O_6]^{4-}$: Sala-Pala, J.; Guerchais, J. E.; Edwards, A. J. *Angew. Chem., Int. Ed. Engl.* **1982**, *21*, 870–871.

(39) Cotton, F. A. *Pure Appl. Chem.* **1967**, *17*, 25.

(40) Summerville, R. H.; Hoffmann, R. *J. Am. Chem. Soc.* **1979**, *101*, 3821–3831.

(41) (a) Suzuki, M.; Murata, S.; Uehara, A.; Kida, S. *Chem. Lett.* **1987**, 281–284. (b) Dismukes, G. C.; Sheats, J. E.; Smegal, J. A. *J. Am. Chem. Soc.* **1987**, *109*, 7202–7203. (c) Mabad, B.; Tuchagues, J.-P.; Hwang, Y. T.; Hendrickson, D. N. *J. Am. Chem. Soc.* **1985**, *107*, 2801–2802. (d) Diril, H.; Chang, H.-R.; Zhang, X.; Larsen, S. K.; Potenza, J. A.; Pierpont, C. G.; Schugar, H. J.; Isied, S.S.; Hendrickson, D. N. *J. Am. Chem. Soc.* **1987**, *109*, 6207–6208.

(42) (a) Morrison, M. M.; Sawyer, D. T. *J. Am. Chem. Soc.* **1977**, *99*, 257. (b) Yamaguchi, K. S.; Sawyer, D. T. *Isr. J. Chem.* **1985**, *25*, 164–176. (c) Cooper, S. R.; Calvin, M. *J. Am. Chem. Soc.* **1977**, *99*, 6623.

(43) Christmas, C.; Vincent, J. B.; Huffmann, J. C.; Christou, G.; Chang, H.-R.; Hendrickson, D. N. *J. Chem. Soc., Chem. Commun.* **1987**, 1303–1305.

(44) Armstrong, W. H.; Lippard, S. J. *J. Am. Chem. Soc.* **1984**, *106*, 4632–4633.

(45) (a) Reem, R. C.; Solomon, E. I. *J. Am. Chem. Soc.* **1984**, *106*, 8323–8325. (b) Reem, R. C.; Solomon, E. I. *J. Am. Chem. Soc.* **1987**, *109*, 1216–1226.

(46) (a) Kennedy, B. J.; Murray, K. S. *Inorg. Chem.* **1985**, *24*, 1552–1557. (b) Kennedy, B. J.; Murray, K. S. *Inorg. Chem.* **1985**, *24*, 1557–1560.

(47) This program has been written by J. Bonvoisin and E. P. Day (University of Minneapolis).

(48) Ménage, S.; Girerd, J. J.; Gleizes, A. *J. Chem. Soc., Chem. Commun.* **1988**, 431.

(49) (a) Armstrong, W. H.; Lippard, S. J. *J. Am. Chem. Soc.* **1983**, *105*, 4837–4838. (b) Armstrong, W. H.; Spool, A.; Papaefthymiou, G. C.; Frankel, R. B.; Lippard, S. J. *J. Am. Chem. Soc.* **1984**, *106*, 3653–3667. (c) Toftlund, H.; Murray, K. S.; Zwack, P. R.; Taylor, L. F.; Anderson, O. P. *J. Chem. Soc., Chem. Commun.* **1986**, 191–193.

(50) Kahn, O. *Angew. Chem., Int. Ed. Engl.* **1985**, *24*, 834–850.

(51) Cooper, S. R.; Dismukes, G. C.; Klein, M. P.; Calvin, M. *J. Am. Chem. Soc.* **1978**, *100*, 7248–7252.

(52) (a) Camenzind, M. J.; Hollander, F. J.; Hill, C. L. *Inorg. Chem.* **1982**, *21*, 4301–4308. (b) Pavacik, P. S.; Huffman, J. C.; Christou, G. *J. Chem. Soc., Chem. Commun.* **1986**, 43–44.

(53) Zimmermann, R.; Spiering, H.; Ritter, G. *Chem. Phys.* **1974**, *4*, 133–141.

(54) Abragam, A.; Bleaney, B. *Electron Paramagnetic Resonance of Transition Ions*; Dover: New York, 1986.

(55) We would like to point out that our data do not allow an unambiguous determination of *J* and *D* because they are recorded in low field and the temperature was only varied down to 2.9 K. Higher field and lower temperature data are required to evaluate definitive numbers.

Table X. Comparison of Parameters of the $M(\mu\text{-}X)_3M$ Core (x = OH, O) in Confacial Bioctahedral Complexes (Distances and Angles Are Average Values)

complex	ref	M—O, Å	O···O, Å	O—M—O, deg	M—O—M, deg	M···M, Å
$[L'Cr(\mu\text{-}OH)_3CrL']^{3+}$	*a*	1.972	2.54	80.1	84.1	2.642
$[(NH_3)_3Cr(\mu\text{-}OH)_3Cr(NH_3)_3]^{3+}$	*b*	1.976	2.55	79.9	83.5	2.631
$[(NH_3)_3Co(\mu\text{-}OH)_3Co(NH_3)_3]^{3+}$	*c*	1.930	2.50	80.7	83.3	2.565
$[L'Mn(\mu\text{-}O)_3MnL']^{2+}$	*d*	1.822	2.45	84.6_5	78.1	2.296
$[(ttp)Nb(\mu\text{-}O)_3Nb(ttp)]$	*e*	1.87	2.20	71.9	94.3	2.75

[a] Reference 21. [b] Andersen, P.; Døssing, A.; Larsen, S.; Pedersen, E. *Acta Chem. Scand.* **1987**, *A41*, 381–390. [c] Thewalt, U. *Z. Anorg. Allg. Chem.* **1975**, *412*, 29–36. [d] This work. [e] Reference 56b.

Table XI. Electronic Spectra[a] of Complexes

complex	λ_{max}, nm (ϵ, L mol^{-1} cm^{-1})
1·$(ClO_4)_2$	232 (3.4×10^3), 280 (3.8×10^3), 495 (324), 520 (250), 545 (sh), 560 (sh), 570 (sh), 665 (95), 910 (40)
2·$(ClO_4)_2$·H_2O	250 (sh), 300 (1.4×10^4), 486 (667), 521 (638), 720 (104), 1000 (63)
6·$(ClO_4)_3$	340 (1.8×10^4), 523 (1.1×10^3), 700 (sh), 780 (sh), 1400 (100)
7[b]	450, 610, 1000 (sh)
8·Br_4·$5.5H_2O$	336 (1.7×10^4), 552 (2.6×10^3), 770 (sh), 1010 (256)
9·$(PF_6)_2$·H_2O	238 (1.8×10^4), 271 (1.6×10^4), 315 (9.4×10^3), 394 (1.3×10^3), 470 (sh)
$L'MnCl_3$	226 (6.3×10^3), 293 (6.5×10^3), 412 (1.37×10^3), 562 (519)
$L'Mn(NCS)_3$	340 (sh), 397 (6.3×10^3), 549 (607)
$L'Mn(N_3)_3$	240 (1.05×10^4), 343 (7.9×10^3), 427 (5.0×10^3), 620 (sh)

[a] Measured in acetonitrile at 20 °C (ϵ are per dimer or tetramer; except those of $L'MnX_3$). [b] Reflectance spectrum.

Cr) as summarized in Table X. Here also no metal–metal bonding occurs. On the other hand, a very interesting structure of one other tri-μ-oxo bridged complex has been reported, namely $[\{Nb(tpp)\}_2(\mu\text{-}O)_3]$ (tpp = 5,10,15,20-tetraphenylporphyrinate).[56] The average $Nb\text{–}O_{oxo}$ bond distance is 1.87 Å, which is slightly longer (by 0.05 Å) than the corresponding bond length in **9**, but the Nb···Nb distance of 2.75 Å is longer by 0.454 Å and the average Nb–O–Nb bond angle is 94°. The niobium(V) centers in this complex have a d^0 electronic configuration and, consequently, no Nb···Nb bond can be formed. Interestingly, the effective ionic radii of Mn(IV) and Nb(V) are very similar (0.64 Å).[27] This comparison suggests a bonding Mn–Mn interaction in **9**. It is noted that in the low-temperature phase of $BaMnO_3$ also a short $Mn^{IV}\text{–}Mn^{IV}$ interaction at 2.34 Å has been reported.[57]

We feel that **9** represents an interesting borderline case. The geometry of the $\{Mn(\mu\text{-}O)_3Mn\}^{2+}$ core enforces a close contact of the Mn^{IV} ions leading to partial spin pairing (μ_{eff}(100 K) = 0.32 μ_B per dimer and 0.84 μ_B at 300 K), which may involve a metal–metal bond.

Electronic Spectra. The absorption spectra of **1** and **2** in acetonitrile at ambient temperature and the spectrum reported for (μ-oxo)bis(μ-acetato)bis[hydrotris(pyrazolylborate)manganese(III)][8] are very similar. In the visible range these three spectra are also quite similar to those published for a manganese catalase of *Lactobacillus plantarum*[5] and for a ribonucleotide reductase of *Brevibacterium ammoniagenes*.[4c] They are supportive to the idea that a (μ-oxo)bis(μ-carboxylato)dimanganese(III) structural unit occurs in these biomolecules.

Table XI summarizes the data of all spectra measured and Figure 7 shows the spectrum of **9** in acetonitrile. Interestingly, the spectra of **8** and **9** are very different despite common *fac*-$N_3O_3Mn^{IV}$ chromophores in both complexes. This may be interpreted as further evidence for a Mn···Mn interaction in **9** that is not present in **8**.

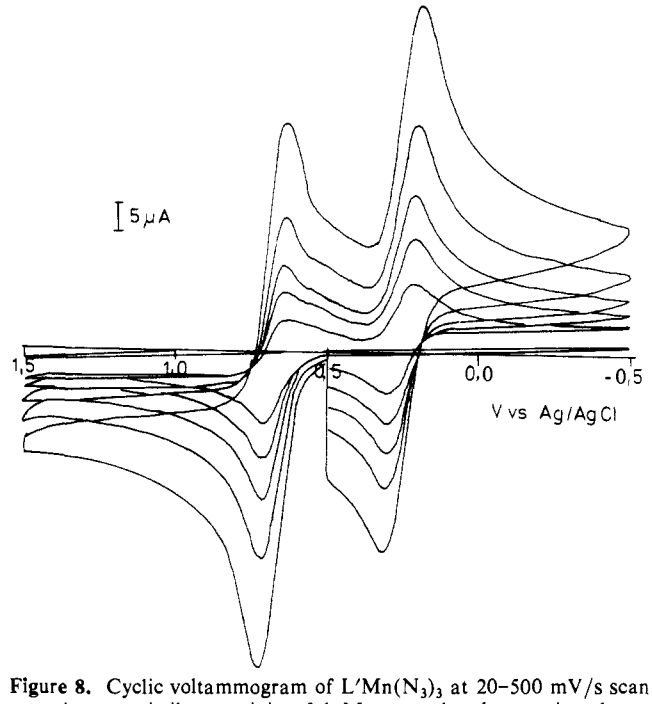

Figure 8. Cyclic voltammogram of $L'Mn(N_3)_3$ at 20–500 mV/s scan rates in acetonitrile containing 0.1 M tetra-*n*-butylammonium hexafluorophosphate.

Electrochemistry. A cyclic voltammogram (CV) of $L'Mn(N_3)_3$ in acetonitrile in the potential range +1.5 to −0.5 V vs Ag/AgCl with tetra-*n*-butylammonium hexafluorophosphate ($TBAPF_6$) as supporting electrolyte (Figure 8) displays a reversible one-electron wave with $E_{1/2}$ = +0.15 V vs Fc^+/Fc, corresponding to formation of $[L'Mn(N_3)_3]^+$ and a quasireversible one-electron-transfer reaction with $E_{1/2}$ = −0.27 V vs Fc^+/Fc, corresponding to the formation of $[L'Mn(N_3)_3]^-$. Similar behavior has been observed for $L'MnCl_3$ with redox potentials at +0.68 and +0.10 V vs Fc^+/Fc. Thus these two mononuclear complexes of Mn^{III} may be reduced to Mn^{II} and oxidized to Mn^{IV} (eq 1). The reduced

$$[L'Mn^{II}X_3]^- \underset{+e^-}{\overset{-e^-}{\rightleftharpoons}} L'Mn^{III}X_3 \underset{+e^-}{\overset{-e^-}{\rightleftharpoons}} [L'Mn^{IV}X_3]^+ \qquad (1)$$

$$(X = (N_3), Cl^-)$$

forms $[L'MnX_3]^-$ slowly decompose presumably with formation of neutral five-coordinate species $L'Mn^{II}X_2$. Chemically, $L'MnCl_3$ oxidizes ferrocene to afford a deep blue solution of the ferrocenium cation and colorless $[L'MnCl_3]^-$. $L'Mn(N_3)_3$ does not react with ferrocene.

The electrochemistry of **1** and **2** has been briefly described in ref 7 and 9. The CV of the hexafluorophosphate salt of **2** in acetonitrile at 25 °C, containing $TBAPF_6$ as supporting electrolyte, in the potential range 0 to 1.5 V vs Fc^+/Fc exhibits a reversible one-electron wave at $E_{1/2}$ = +0.58$_5$ V vs Fc^+/Fc and a second reversible one-electron wave at $E_{1/2}$ = −0.53 V vs Fc^+/Fc (Figure 9B). Controlled-potential coulometry at +0.65 and 0.0 V vs Fc^+/Fc established a one-electron-transfer process in both cases. An identical CV was obtained when **6** was used as starting material. These CVs are only obtained if the presence of water is rigorously excluded. For instance, when the perchlorate salt of

(56) (a) Johnson, J. F.; Scheidt, R. *Inorg. Chem.* **1978**, *17*, 1280. (b) Lecomte, C.; Protas, J.; Guilard, B. F.; Fournari, P. *J. Chem. Soc., Dalton Trans.* **1979**, 1306.
(57) Hardy, A. *Acta Crystallogr.* **1962**, *15*, 179.

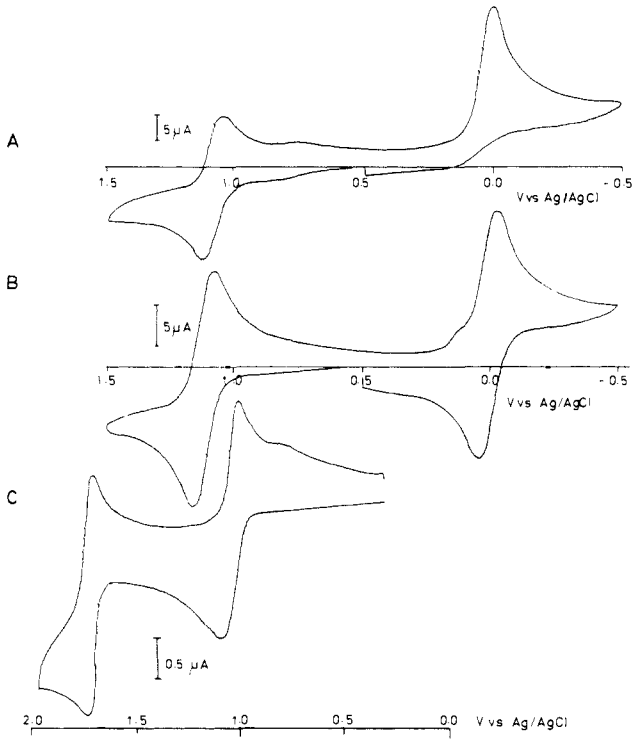

Figure 9. CVs of **2**: (A) CV for **2**·$(ClO_4)_2$·H_2O in acetonitrile containing 0.1 M $TBAPF_6$ at 100 mV/s scan rate (working electrode: Pt-button). (B) CV of **2**·$(PF_6)_2$ in acetonitrile (0.1 M $TBAPF_6$) at 100 mV/s scan rate (working electrode: Pt-button). (C) CV of **2**·$(PF_6)_2$ in liquid SO_2 (−40 °C; 0.1 M $TBAPF_6$) at 50 mV/s scan rate (working electrode: Pt-button).

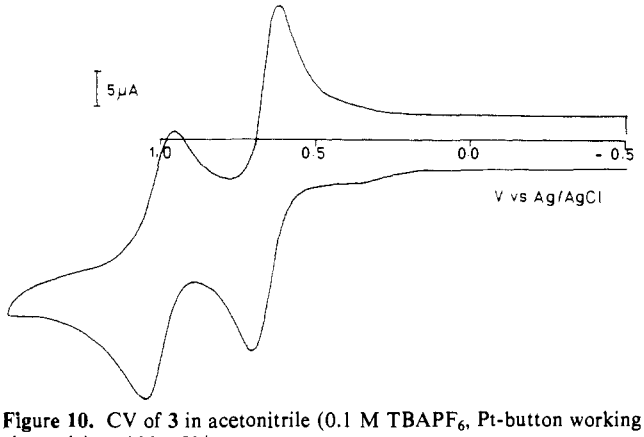

Figure 10. CV of **3** in acetonitrile (0.1 M $TBAPF_6$, Pt-button working electrode) at 100 mV/s scan rate.

2 was used, which contains one molecule of water of crystallization per dimer, the more cathodic wave becomes irreversible (Figure 9A), whereas the anodic wave remains unchanged. The same behavior (Figure 9A) was observed when a drop of water was added to a solution of **2**·$(PF_6)_2$. These results indicate the formation of $Mn^{III}Mn^{IV}$ and $Mn^{II}Mn^{III}$ mixed-valent μ-oxo bridged dimers, respectively (eq 2). In the presence of water the oxo-bridged $Mn^{II}Mn^{III}$ species is unstable.

$$[L'_2Mn^{III}Mn^{IV}(\mu\text{-}O)(\mu\text{-}CH_3CO_2)_2]^{3+} \underset{-e^-}{\overset{+e^-}{\rightleftharpoons}} [L'_2Mn^{III}_2(\mu\text{-}O)(\mu\text{-}CH_3CO_2)_2]^{2+} \underset{-e^-}{\overset{+e^-}{\rightleftharpoons}} [L'_2Mn^{II}Mn^{III}(\mu\text{-}O)(\mu\text{-}CH_3CO_2)_2]^{+} \quad (2)$$

At even more positive potentials (>1.0 V vs Fc^+/Fc) a further quasireversible one-electron wave has been detected, although the stability of this strongly oxidizing species (an Mn^{IV}_2 dimer) is low in acetonitrile. With use of the more redox-inert solvent liquid SO_2[9] at −40 °C two reversible one-electron processes have been observed (Figure 9C) that correspond to the formation of **6** ($E_{1/2}$ = +0.55 V vs Fc^+/Fc) and its dimeric Mn^{IV}_2 analogue ($E_{1/2}$ = 1.21 V vs Fc^+/Fc).

$$[L'_2Mn^{III}Mn^{IV}(\mu\text{-}O)(\mu\text{-}CH_3CO_2)_2]^{3+} \underset{+e^-}{\overset{-e^-}{\rightleftharpoons}} [L'_2Mn^{IV}_2(\mu\text{-}O)(\mu\text{-}CH_3CO_2)_2]^{4+} \quad (3)$$

The CV of the hydroxo-bridged species **3** exhibits one quasireversible one-electron transfer wave in the potential range −0.5 to +0.5 V vs Ag/AgCl ($E_{1/2}$ = +0.15 V vs Fc^+/Fc) that corresponds to the formation of a hydroxo-bridged $Mn^{II}Mn^{III}$ mixed-valent complex. Such species have recently attracted much attention, and a number of (μ-phenoxy)bis(μ-acetato)dimanganese(II/III) compounds have been isolated[41] and one compound has been characterized by X-ray crystallography.[41] In the present case it has not been possible to isolate the oxidized form of **3**.

At more positive potentials a further quasireversible one-electron-transfer wave has been observed at $E_{1/2}$ = +0.50 V vs Fc^+/Fc that corresponds to the formation of a hydroxo-bridged $Mn^{III}Mn^{III}$ species (Figure 10) (eq 4). Although it has not been

$$[L'Mn^{II}_2(\mu\text{-}OH)(\mu\text{-}CH_3CO_2)_2]^{+} \underset{+e^-}{\overset{-e^-}{\rightleftharpoons}} [L'_2Mn^{II}Mn^{III}(\mu\text{-}OH)(\mu\text{-}CH_3CO_2)_2]^{2+} \underset{+e^-}{\overset{-e^-}{\rightleftharpoons}} [L'_2Mn^{III}_2(\mu\text{-}OH)(\mu\text{-}CH_3CO_2)_2]^{3+} \quad (4)$$

possible to isolate the μ-hydroxo-bridged manganese(III) dimer, such a species has been characterized for a (μ-oxo)bis(μ-acetato)diiron(III) complex,[44] and we suggest the following equilibrium in aqueous solution, eq 5, to exist. This acid–base

$$[L'_2Mn^{III}_2(\mu\text{-}O)(\mu\text{-}CH_3CO_2)_2]^{2+} + H^+ \rightleftharpoons [L'_2Mn^{III}_2(\mu\text{-}OH)(\mu\text{-}CH_3CO_2)_2]^{3+} \quad (5)$$

equilibrium together with the known electrochemistry of both species allows an understanding of the observed disproportionation of **2** in the presence of protons. The protonated form of **2** (hydroxo-bridged) is only a slightly weaker oxidant in acetonitrile (by 80 mV) than the deprotonated form (oxo-bridged). In aqueous solution this may be the other way around and the following redox reaction may be thermodynamically favorable in acidic aqueous solution, eq 6, yielding **6** and manganese(II). These studies show

$$Mn^{III}\text{—}O\text{—}Mn^{III} + Mn^{III}\text{—}OH\text{—}Mn^{III} \rightarrow Mn^{II}\text{—}OH\text{—}Mn^{III} + Mn^{III}\text{—}O\text{—}Mn^{IV} \quad (6)$$

$$\downarrow$$

decomposition

that it is possible to chemically or electrochemically generate dimeric manganese model complexes at various oxidation levels without changing dramatically the overall structure of these dimers. Simple electron-transfer reactions and an occasional protonation–deprotonation reaction at an oxo- or hydroxo-bridge occur in a readily accessible potential range. This type of chemistry mimics the known properties of the manganese-containing active site in PS II where the S_{0-2} states have been shown to correspond to successive one-electron oxidations that occur without gross changes of the overall structure of this cluster. The electrochemistry of complexes **2** and **3** resembles in some respects the one described by Sawyer and co-workers for the $[Mn_2O_2(phen)_4]^{n+}$ system.[42]

The electrochemistry of the perchlorate salt of **8** and **9** is uneventful. Acetonitrile solutions of these compounds show no electron-transfer process in the potential range −1.5 to +2.0 V vs Ag/AgCl. This is somewhat surprising considering that the manganese centers are in the oxidation state +IV. Mixed-valent manganese(III/IV) tetranuclear species are proposed to play an important role in the water oxidation process of PS II and tetranuclear mixed-valent model compounds begin to appear in the literature.[15,43]

Magnetic Studies. Measurements were carried out on solid samples with a Faraday-type magnetometer. Numerical values of μ_{eff} and spin exchange coupling constants for complexes under investigation are summarized in Table XII.

Table XII. Magnetic Properties of Complexes

complex	μ_{eff}(298 K)	J, cm^{-1}
L'MnCl$_3$	5.28 (2)	
L'MnBr$_3$	5.06 (2)	
L'Mn(N$_3$)$_3$	5.16 (2)	
L'Mn(NCS)$_3$	5.00 (2)	
2·(ClO$_4$)$_2$·H$_2$O		+18
3·(ClO$_4$)		−18
4·[BPh$_4$]		−3.5
5·[BPh$_4$]$_2$·CH$_3$CN		−440
6·(ClO$_4$)$_3$		−80
7	see text	
8	see text	ferromagnetic coupling
9		−780

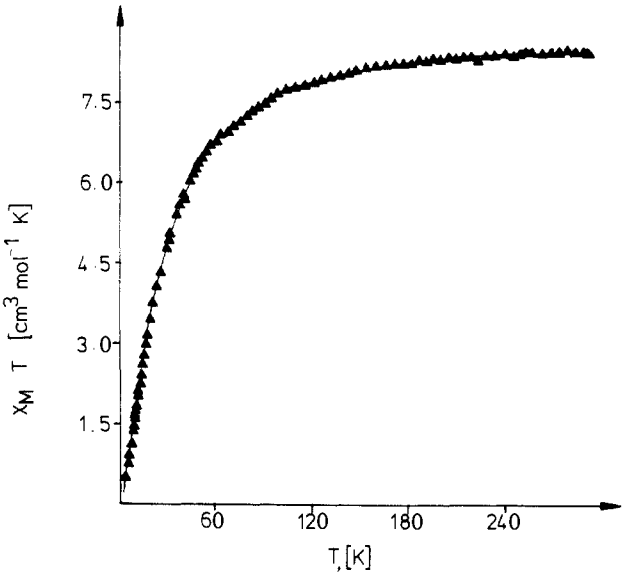

Figure 11. Plot of χ_M·T vs T for **4**. The solid line represents the best fit of data according to eq 7.

For the monomeric compounds L'MnX$_3$ (X = Cl, Br, N$_3$, NCS) magnetic moments (5.0–5.28 μ_B) were found to be independent of the temperature (100–293 K). They are as expected for high-spin (d^4) octahedral complexes of manganese(III).

The magnetic susceptibility of the binuclear tris(μ-acetato)-dimanganese(II) complex **4** has been measured from room temperature to 3.4 K. Figure 11 shows χ_M·T as a function of T. The product χ_M·T decreases from 8.43 cm^3 mol^{-1} K at 291.7 K to 0.51 cm^3 mol^{-1} K at 3.4 K, which is characteristic of an antiferromagnetic spin exchange between the two high-spin Mn^{II} centers of the cation in **4**. A plot of χ_M vs T exhibits a maximum at 10 K.

To fit the data we used a simple Heisenberg hamiltonian, eq 7, because (i) the zero-field-splitting (ZFS) for Mn^{II} is much

$$\chi_M = \frac{N\beta^2 g^2}{3k\cdot T} \frac{\sum_{S=0}^{5} S(S+1)(2S+1)e^{-E(S)/k\cdot T}}{\sum_{S=0}^{5} (2S+1)e^{-E(S)/k\cdot T}} \qquad (7)$$

smaller than that for Mn^{III} and (ii) the magnetic susceptibility is less sensitive to ZFS in the antiferromagnetic case than in the ferromagnetic case where $E(S) = -J/2S(S+1)$ and the other constants have their usual meaning. The best fit was obtained for $J = -3.5$ cm^{-1} and $g = 2.025$. The small difference between this g value and $g = 2.00$ expected for Mn^{II} is inside experimental uncertainties. The agreement factor R of 4×10^{-5} is excellent, where $R = [\sum(\chi_M^{exp} - \chi_M^{calc})^2]/\sum(\chi_M^{exp})^2$.

For the (μ-hydroxo)bis(μ-acetato)dimanganese(II) complex **3** a significantly stronger intramolecular antiferromagnetic coupling ($H = -JS_1S_2$; $S_1 = S_2 = {}^5/_2$; $g = 2.00$; $J = -18$ cm^{-1}) has been reported previously.[9] These results nicely corroborate results for the corresponding model compounds of deoxyhemerythrin where

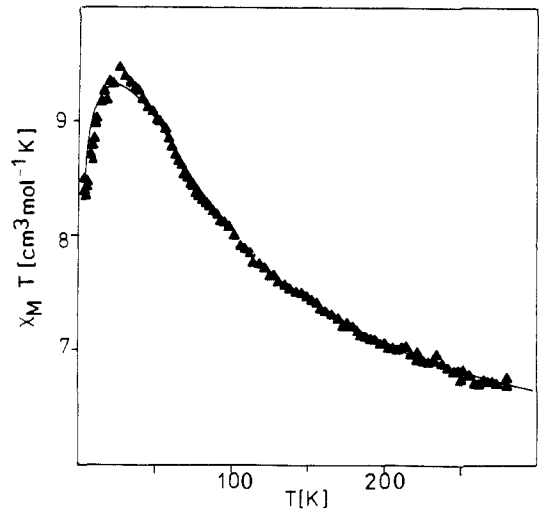

Figure 12. Plot of χ_M·T vs T for **2**·(BPh$_4$)$_2$. The solid line represents the best fit of data according to eq 8.

the biomolecule and the model [L'$_2$Fe$_2$(μ-OH)(μ-CH$_3$CO$_2$)$_2$]-(ClO$_4$) exhibit antiferromagnetic spin exchange coupling ($J = -26$ cm^{-1}).[28,45] The absence of a hydroxo bridge in **4** leads to a much smaller antiferromagnetic coupling.

The magnetic susceptibilities of the perchlorate monohydrate and tetraphenylborate salts of **2** were studied from room temperature to 2.5 K. The results for both salts are within experimental error identical. Figure 12 shows the product χ_M·T vs T for **2**·(BPh$_4$)$_2$. χ_M·T per binuclear manganese(III) unit increases from 6.69 cm^3 mol^{-1} K (5.17 μ_B/Mn) at 281.4 K to 9.47 cm^3 mol^{-1} K at 26.6 K and decreases then to 8.38 cm^3 mol^{-1} K at 2.9 K. The increase of χ_M·T with decreasing temperature is characteristic of a ferromagnetic coupling between the two high-spin Mn^{III} ions in **2**. The value for μ_{eff}/Mn at room temperature of **2** is larger than the reported one for the hydro-tris(pyrazolyl)borate analogue[8] (μ_{eff}/Mn = 4.89 μ_B) where no coupling between the Mn centers was found.

At low temperatures the product χ_M·T of **2** does not reach the predicted value of 10 cm^3 mol^{-1} K for an $S = 4$ ground state. ZFS[46] and intermolecular interactions between cations in the solid state may be responsible for this behavior. The latter point is believed to contribute very little, because changing the bulkiness of the counteranion in **2** on going from perchlorate to tetraphenylborate did not affect the susceptibility measurably. Therefore, we have fitted the data taking into account only ZFS and intradimer exchange coupling by using the spin Hamiltonian given in eq 8. A program[47] was written to find the energy levels

$$H = -J\vec{S}_1\vec{S}_2 + \vec{S}_1D_1\vec{S}_1 + \vec{S}_2D_2\vec{S}_2 + \beta\vec{H}g_1S_1 + \beta\vec{H}g_2S_2 \qquad (8)$$

as a function of the magnetic field. The best fit obtained for 1 kG is shown in Figure 12 with $J = +18$ cm^{-1}, $D_1 = D_2 = 3$ cm^{-1}, and $g_{1,\parallel} = g_{2,\parallel} = 2.00$. E_1 and E_2 have been set to zero. The value of $g_1 = g_2 = 1.925$ is obtained from the second-order perturbation expression in ref 53

$$g_\perp = g_\parallel - 2D/\lambda$$

where λ is the spin–orbit coupling constant. We took λ as 80 cm^{-1} from ref 54.[55]

The observation of an intramolecular ferromagnetic coupling **2** is remarkable, since in the analogous complex of Lippard and Dismukes[8] the Mn^{III} ions are uncoupled, and in [(bpy)$_2$-(H$_2$O)$_2$Mn$^{III}_2$(μ-O)(μ-CH$_3$CO$_2$)$_2$](PF$_6$)$_2$·H$_2$O$_{1.75}$[48] weak antiferromagnetic coupling has recently been observed ($J = -6.8$ cm^{-1}). Obviously, the {Mn$^{III}_2$(μ-O)(μ-CH$_3$CO$_2$)$_2$}$^{2+}$ core has two magnetic characteristics in comparison with the magnetic properties of the strongly antiferromagnetically coupled {Fe$^{III}_2$(μ-O)(μ-CH$_3$CO$_2$)$_2$}$^{2+}$ core:[28,49] (i) the coupling is small and (ii) the sign of the coupling depends on the nature of the terminal capping ligands. The former fact has been interpreted[8] as follows: the d_{z^2} orbitals are directed along the M–O$_{oxo}$ bond vectors; they are occupied in the high-spin

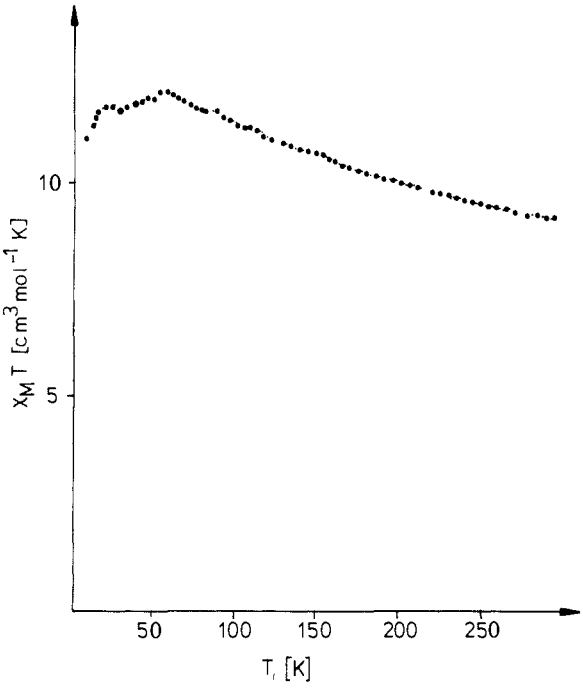

Figure 13. Plot of $\chi_M \cdot T$ vs T for **8**.

d^5 Fe(III) compounds but are unoccupied in the high-spin d^4 Mn(III) complexes, whereby the major pathway for orbital coupling is eliminated. The rationalization of observation (ii) is more difficult and requires a detailed analysis of all possible orbital contributions. The Mn^{III}–O–Mn^{III} bond angle is different in the above Mn^{III}_2 dimers. It may decisively determine the sign of the exchange coupling, as has been demonstrated convincingly for the hydroxo-bridged copper(II) dimers.[58] Second, it is known that external ligands can play a role on the sign and magnitude of exchange coupling in dimers.[50]

Removal of one electron from **2** yields the mixed-valent $Mn^{III}Mn^{IV}$ dimer **6** (see above), which has been characterized by X-ray crystallography and whose magnetic properties have been investigated previously. **6** possesses an $S = {}^1/_2$ ground state, and the two manganese centers (Mn^{III} d^4 and Mn^{IV} d^3) are moderately strongly antiferromagnetically coupled ($J = -80$ cm^{-1}).[9] In contrast, in the mixed-valent dimer **5** containing the $\{Mn^{III}(\mu\text{-}O)_2(\mu\text{-}CH_3CO_2)Mn^{IV}\}^{2+}$ core very strong antiferromagnetic coupling ($J = -440$ cm^{-1}) has been observed as well as an $S = {}^1/_2$ ground state,[10] which is in good agreement with other complexes containing the $\{Mn^{III}Mn^{IV}(\mu\text{-}O)_2\}^{3+}$ core.[29,51]

The average effective magnetic moment per manganese of **7** decreases from 4.6 μ_B at 293 K to 4.4 μ_B at 120 K. If we assume (i) a strong antiferromagnetic coupling between the Mn(IV) centers in the dimeric cation to be of the same magnitude as in other complexes containing the $[Mn^{IV}_2O_2]^{4+}$ moiety[29] (2.0 μ_B per dimer at 293 K and 0.75 at 120 K) and that (ii) the Mn(II) centers in the polymeric anion are not coupled (d^5 high spin; 5.7 μ_B/Mn^{II}), an average effective magnetic moment of 4.78 μ_B/Mn at 293 K and of 4.46 μ_B/Mn at 120 K is calculated. These calculated values are quite close to the experimental values considering the crudeness of this model, and they do corroborate the assignment of oxidation states in **7** as +IV in the dimeric cation and +II in the anion.

The magnetic susceptibility of the tetranuclear manganese(IV) complex **8** was measured from room temperature to 7.5 K. Figure 13 shows the measured values $\chi_M \cdot T$ vs T. The product $\chi_M \cdot T$ at 295.1 K is 9.106 cm^3 mol^{-1} K and increases to 11.553 cm^3 mol^{-1} K at 84.9 K and decreases then to 10.902 cm^3 mol^{-1} K at 7.5 K. The effective magnetic moment per Mn at 295 K is 4.27 μ_B, which is slightly larger than values reported for monomeric octahedral complexes of manganese(IV).[52] The behavior at temperatures

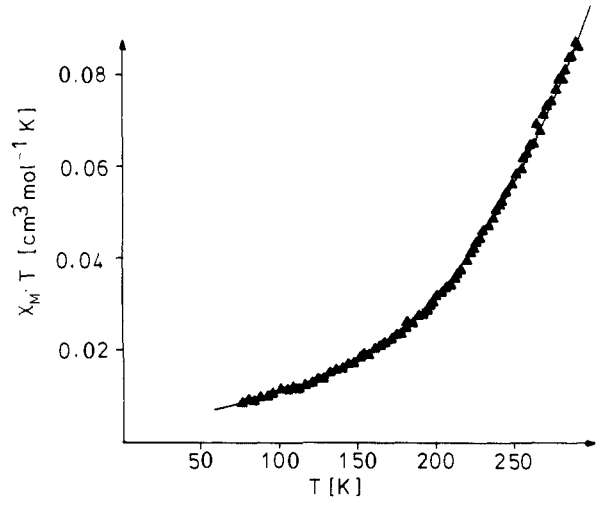

Figure 14. Plot of $\chi_M \cdot T$ vs T for **9**. The solid line represents the best fit of data according to eq 9.

>84.9 K indicates a small ferromagnetic exchange coupling in the tetranuclear cation in **8**. Since the cluster is rather symmetric (adamantane $\{Mn_4O_6\}^{4+}$ skeleton) all six J_{ij} constants are expected to be close to each other. ZFS and, possibly, intertetramer coupling prevent the magnetic susceptibility from attaining the hypothetical value for an $S = 6$ ground state ($\chi_M \cdot T = 21$ cm^3 mol^{-1} K).

Contrasting the weak ferromagnetic coupling in **8**, a very strong intradimer antiferromagnetic exchange coupling is observed in **9**. Figure 14 shows the data after correction for underlying diamagnetism as $\chi_M \cdot T$ vs T. The paramagnetism is very low and indicative of a strong antiferromagnetic coupling within the dimer. The product $\chi_M \cdot T = 0.087$ at 289.8 K and *decreases* with decreasing T. This behavior is characteristic of an $S = 0$ ground state with an excited magnetic state at an energy Δ. We used the following expression, eq 9, which is valid for an excited triplet

$$\chi_M \cdot T = \frac{Ng^2\beta^2}{k}(1-p)\frac{2}{3+\exp\left(\frac{\Delta}{k \cdot T}\right)} + p \cdot C + \text{TIP} \quad (9)$$

state, where g refers to the triplet state, p is the amount of Curie law impurity, $C = (Ng^2\beta^2/3k)^3/_2(^3/_2 + 1)$ is the Curie constant of this impurity which is considered to be a monomeric Mn(IV) species, and TIP is temperature-independent paramagnetism for Mn(IV) ions. The latter two quantities can be ignored for strong paramagnetic systems but are important for materials exhibiting very weak paramagnetism. Our best fit was obtained with $g = 2.0$; $\Delta = 780$ cm^{-1}; $p = 0.03\%$ and TIP = 98×10^{-6} cm^3 mol^{-1}. Using an expression for an $S = {}^3/_2$ dimer ($H = -J \cdot S_1S_2$) leads to the same result ($\Delta = -J = 780$ cm^{-1}) because the data correspond to no population of $S = 2$ and $S = 3$ states.

Summary and Conclusions

A series of binuclear complexes containing a (μ-oxo)bis(μ-acetato)dimanganese or a (μ-hydroxo)bis(μ-acetato)dimanganese core and a tridentate *N,N',N''*-trimethyl-1,4,7-triazacyclononane capping ligand at each manganese center have been synthesized. Their reactivity and electronic and magnetic properties have been studied. The electrochemistry of these compounds provides a basis for understanding the redox behavior of the manganese-containing active site in photosystem II. Thus in a series of successive one-electron steps the oxidation level of the manganese centers may be varied from +II to +IV without changing the gross overall structure of the compounds. Mixed-valent species $Mn^{II}Mn^{III}$ and $Mn^{III}Mn^{IV}$ have been characterized electrochemically and in the case of the latter have been isolated. Disproportionation reactions of the $\{Mn^{III}_2(\mu\text{-}O)(\mu\text{-}CH_3CO_2)_2\}^{2+}$ unit in the presence of protons have been investigated.

From its electronic spectrum it has been concluded[8] that the binuclear $\{Mn^{III}_2(\mu\text{-}O)(\mu\text{-}CH_3CO_2)_2\}^{2+}$ core occurs in a pseudo-

(58) McGregor, K. T.; Watkins, N. T.; Lewis, D. L.; Drake, R. F.; Hodgson, D. J.; Hatfield, W. E. *J. Inorg. Nucl. Chem. Lett.* **1973**, *9*, 423.

catalase isolated from *Lactobacillus plantarum* and in a recently characterized ribonucleotide reductase from *Brevibacterium ammoniagenes*.[4c]

Oxidation reactions of species containing LMn^{III} or $L'Mn^{III}$ units in alkaline aqueous solution in the presence of oxygen afford the tetranuclear $[L_4Mn_4(\mu\text{-}O)_6]^{4+}$ and the dimeric $[L'_2Mn_2(\mu\text{-}O)_3]^{2+}$ cations, respectively, which contain manganese(IV) centers. In the latter complex the unprecedented short $Mn^{IV}\cdots Mn^{IV}$ distance and its magnetic properties may indicate the presence of a bonding interaction between the two manganese(IV) centers, but the data at hand do not allow an unambiguous assignment. This compound represents a fascinating borderline case.

Acknowledgment. This work was supported by the Deutsche Forschungsgemeinschaft and the Fonds der Chemischen Industrie. We thank Drs. A. Neves, K. Pohl and E. Wasielewska for their help with the cyclic voltammetric measurements.

Supplementary Material Available: Lists of bond distances, bond angles, and anisotropic displacement parameters and calculated positional parameters for hydrogen atoms (Tables S2-14) of complexes **4**, **7**, **8**, and **9**, positional and isotropic thermal parameters of the BPh_4 anion in **4** (Table S1), and magnetic susceptibility data for **8** (Table S14) (22 pages). Ordering information is given on any current masthead page.

The Dynamics of Reaction of a Water-Soluble and Non-μ-Oxo Dimer Forming Iron(III) Porphyrin with *tert*-Butyl Hydroperoxide in Aqueous Solution. 1. Studies Using a Trap for Immediate Oxidation Products

John R. Lindsay Smith,† P. N. Balasubramanian, and Thomas C. Bruice*

Contribution from the Department of Chemistry, University of California at Santa Barbara, Santa Barbara, California 93106. *Received March 28, 1988*

Abstract: A kinetic and product study has been carried out in aqueous solution for the reaction of *t*-BuOOH with the water-soluble and non-μ-oxo dimer forming (5,10,15,20-tetrakis(2,6-dimethyl-3-sulfonatophenyl)porphinato)iron(III) hydrate ((**1**)$Fe^{III}(X)$; where X = H_2O or HO^-). Reactions were studied at 30 °C and μ = 0.22 (with $NaNO_3$) between pH 2.22 and 12.96, and the course of reaction was followed by employing the water-soluble 2,2'-azinobis(3-ethylbenzthiazoline-6-sulfonate) (ABTS) as a trap for oxidant intermediates. One-electron oxidation of ABTS provides the chromophoric radical cation $ABTS^{\bullet+}$ (λ_{max} 660 nm). Reactions were carried out under the pseudo-first-order conditions of [ABTS] $\gg$ [*t*-BuOOH] $\gg$ [(**1**)$Fe^{III}(X)$] using between 10- and 100-turnovers of the iron(III) porphyrin catalyst. The reaction is first order in both [*t*-BuOOH]$_i$ and [(**1**)$Fe^{III}(X)]_i$, and both initial and first-order rate constants are independent of [ABTS]$_i$, ionic strength, and buffer concentrations (buffers employed and pH values for buffer dilution experiments: $ClCH_2COOH/ClCH_2COO^-$ (pH 3.45), CH_3COOH/CH_3COO^- (pH 4.60), $H_2PO_4^-/HPO_4^{2-}$ (pH 6.87), $H_3BO_3/H_2BO_3^-$ (pH 8.66), and HCO_3^-/CO_3^{2-} (pH 9.13), collidine/collidine·H^+ (6.18, 6.98, 8.15)). It follows that the rate-determining step occurs after ligation of available alkyl hydroperoxide species (*t*-BuOOH and *t*-$BuOO^-$, pK_a = 12.8) with iron(III) porphyrin species ((**1**)$Fe^{III}(H_2O)_2$ and (**1**)$Fe^{III}(H_2O)(OH)$, pK_a = 7.2), and that these reactions are not subject to either general-acid nor general-base catalysis. A plot of the log of the pH dependent second-order rate constant (k_{obsd}/[(**1**)$Fe^{III}(X)$]) vs pH may be fit by an equation (eq 3) containing the sum of four terms (*A*, *B*, *C*, *D*). The equation contains four apparent acid dissociation constants. There are, however, only two acid dissociation constants associated with the reactants. The pH dependence of the reaction may be explained by taking into account the acid dissociations of *t*-BuOOH when ligated to both (**1**)$Fe^{III}(H_2O)$ and (**1**)$Fe^{III}(OH)$. With $Ph(CH_3)_2C\text{-}OOH$ as the hydroperoxide the products are $Ph(CH_3)C{=}O$ and CH_3OH. The product $Ph(CH_3)C{=}O$ establishes the formation of $Ph(CH_3)_2C\text{-}O^\bullet$ from alkyl hydroperoxide. With *t*-BuOOH the products are $(CH_3)_2C{=}O$ and CH_3OH. When ABTS is used as a trap for intermediate oxidants, the yield of $ABTS^{\bullet+}$ is virtually constant (70%) between pH 4 and 10, assuming two ABTS molecules undergo $1e^-$ oxidation for each *tert*-butyl hydroperoxide moiety reacted. With ABTS the products of *tert*-butyl hydroperoxide decomposition are *t*-BuOH, $(CH_3)_2CO$, and CH_3OH. In the absence of the ABTS trap $(CH_3)_2CO$ (90%) is the predominant product. Increasing concentrations of ABTS result in the yield of $(CH_3)_2CO$ decreasing asymptotically to 15% and the yield of *t*-BuOH increasing to 84%. The following alternate mechanistic proposals have been advanced: (i) The immediate product is the solvent caged species [(**1**)$Fe^{IV}(X)(OH)$-*t*-$BuO^\bullet$] and ~15% of the *t*-$BuO^\bullet$ fragments within the solvent cage to provide $(CH_3)_2CO$ and $CH_3^\bullet$. The *t*-$BuO^\bullet$ which escapes the solvent cage either undergoes the same reaction or is trapped by ABTS depending upon the latter's concentration. Formation of CH_3OH would occur via reaction of $CH_3^\bullet$ with (**1**)$Fe^{IV}(X)(OH)$ much as in the rebound mechanism for hydrocarbon hydroxylation. (ii) In competitive mechanisms 15% of *t*-BuOOH is consumed to provide the caged species [(**1**)$Fe^{IV}(X)(OH)$-*t*-$BuO^\bullet$] accompanied by fragmentation of $(CH_3)_3CO^\bullet$ within the solvent cage etc. The competing reaction would then involve the reduction of the iron(III) porphyrin by the hydroperoxide to form the species (**1**)$Fe^{II}(X)$ + *t*-$BuOO^\bullet$ followed by the rapid conversions 2 *t*-$BuOO^\bullet \rightarrow$ 2 *t*-$BuO^\bullet + O_2$ and O_2 + 2(**1**)$Fe^{II}(X) \rightarrow \rightarrow$ 2(**1**)$Fe^{IV}(O)(X)$.

In previous studies the reaction of hydrogen peroxide with (5,10,15,20-tetrakis(2,6-dimethyl-3-sulfonatophenyl)porphinato)iron(III) and -manganese(III) hydrates ((**1**)$Fe^{III}(X)$ and (**1**)$Mn^{III}(X)$, respectively (where X = H_2O or HO^-)) were investigated in water as a function of pH and buffer acid and base concentrations.[1,2] The pH-dependent second-order rate constants

† Department of Chemistry, University of York, York, England.

(1) Zipplies, M. F.; Lee, W. A.; Bruice, T. C. *J. Am. Chem. Soc.* **1986**, *108*, 4433.

(2) Balasubramanian, P. N.; Schmidt, E. S.; Bruice, T. C. *J. Am. Chem. Soc.* **1987**, *109*, 7865.

0002-7863/88/1510-7411$01.50/0